

Solution-Processable Low-Molecular Weight Extended Arylacetylenes: Versatile p-Type Semiconductors for Field-Effect Transistors and Bulk Heterojunction Solar Cells

Fabio Silvestri,^{†,§} Assunta Marrocchi,^{*,‡} Mirko Seri,[‡] Choongik Kim,[†]
Tobin J. Marks,^{*,†} Antonio Facchetti,^{*,†} and Aldo Taticchi^{*,‡}

Department of Chemistry, the Argonne-Northwestern Solar Energy Research Center, and the Materials Research Center, Northwestern University, 2145 Sheridan Road, Evanston, Illinois 60208-3113, and Department of Chemistry, University of Perugia, Via Elce di Sotto 8, I-06123 Perugia, Italy

Received December 10, 2009; E-mail: assunta@unipg.it (A.M.); t-marks@northwestern.edu (T.J.M.); a-facchetti@northwestern.edu (A.F.); taticchi@unipg.it (A.T.)

Abstract: We report the synthesis and characterization of a series of five extended arylacetylenes, 9,10-bis- $\{[m,p$ -bis(hexyloxy)phenyl]ethynyl}-anthracene (**A-P6t**, **1**), 9,10-bis- $\{[p$ - $\{[m,p$ -bis(hexyloxy)phenyl]ethynyl}phenyl]ethynyl}-anthracene (**PA-P6t**, **2**), 4,7-bis- $\{[m,p$ -bis(hexyloxy)phenyl]ethynyl}-2,1,3-benzothiadiazole (**BTZ-P6t**, **5**), 4,7-bis(5- $\{[m,p$ -bis(hexyloxy)phenyl]ethynyl}thien-2-yl)-2,1,3-benzothiadiazole (**TBTZ-P6t**, **6**), and 7,7'- $\{[m,p$ -bis(hexyloxy)phenyl]ethynyl}-2,1,3-benzothiadiazol-4,4'-ethynyl)-2,5-thiophene (**BTZT-P6t**, **7**), and two arylvinylenes, 9,10-bis- $\{(E)$ - $[m,p$ -bis(hexyloxy)phenyl]vinyl}-anthracene (**A-P6d**, **3**), 9,10-bis- $\{(E)$ - $\{[m,p$ -bis(hexyloxy)phenyl]vinyl}phenyl}vinyl}-anthracene (**PA-P6d**, **4**). Trends in optical absorption spectra and electrochemical redox processes are first described. Next, the thin-film microstructures and morphologies of films deposited from solution under various conditions are investigated, and organic field-effect transistors (OFETs) and bulk heterojunction photovoltaic (OPV) cells fabricated. We find that substituting acetylenic for olefinic linkers on the molecular cores significantly enhances device performance. OFET measurements reveal that all seven of the semiconductors are FET-active and, depending on the backbone architecture, the arylacetylenes exhibit good p-type mobilities (μ up to ~ 0.1 cm² V⁻¹ s⁻¹) when optimum film microstructural order is achieved. OPV cells using [6,6]-phenyl C₆₁-butyric acid methyl ester (PCBM) as the electron acceptor exhibit power conversion efficiencies (PCEs) up to 1.3% under a simulated AM 1.5 solar irradiation of 100 mW/cm². These results demonstrate that arylacetylenes are promising hole-transport materials for p-channel OFETs and promising donors for organic solar cells applications. A direct correlation between OFET arylacetylene hole mobility and OPV performance is identified and analyzed.

Introduction

Semiconducting materials based on π -conjugated organic small molecules and polymers have been extensively investigated for applications in a variety of optoelectronic devices such as light-emitting diodes (OLEDs),¹ field-effect transistors (OFETs),² photovoltaic cells (OPVs),³ sensors, optical amplifiers, and lasers.⁴ One key attraction of organic semiconductors is the tunability of their physical and chemical properties by rational sequential structural modification. Additionally, their

use in place of conventional inorganic semiconductors offers the prospects of low manufacturing costs (i.e., casting or printing technologies using solution-processable materials), large area coverage, and compatibility with flexible substrates. Among

[†] Northwestern University.

[‡] University of Perugia.

[§] Current address: ETH Zürich, Laboratory of Organic Chemistry, Department of Chemistry and Applied Biosciences, HCI G 304 Wolfgang-Pauli-Strasse 10, CH-8093 Zürich, Switzerland.

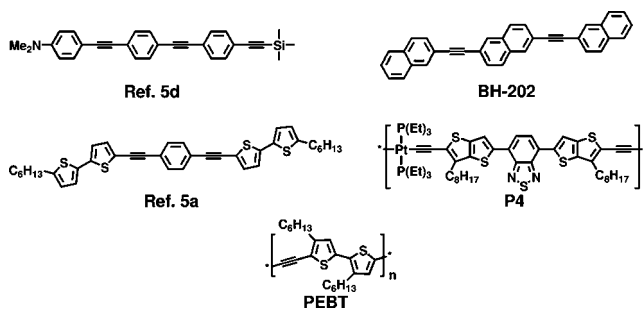
(1) (a) Zhao, L.; Zou, J.-H.; Huang, J.; Li, C.; Zhang, Y.; Sun, C.; Zhu, X.-h.; Peng, J.; Cao, Y.; Roncali, J. *Org. Electron.* **2008**, *9*, 649. (b) Luo, J.; Zhou, Y.; Niu, Z. Q.; Zhou, Q. F.; Ma, Y.; Pei, J. *J. Am. Chem. Soc.* **2007**, *129*, 11314. (c) Perepichka, I. F.; Perepichka, D. F.; Meng, H.; Wudl, F. *Adv. Mater.* **2005**, *17*, 2281. (d) Chen, A. C. A.; Culligan, S. W.; Geng, Y. H.; Chen, S. H.; Klubek, K. P. K.; Vaeth, M.; Tang, C. W. *Adv. Mater.* **2004**, *16*, 783. (e) Oldham, W. J.; Lachicotte, R. J.; Bazan, G. C. *J. Am. Chem. Soc.* **1998**, *120*, 2987. (f) Kraft, A.; Grimsdale, A. C.; Holmes, A. B. *Angew. Chem., Int. Ed.* **1998**, *37*, 402.

(2) (a) Yan, H.; Chen, Z.; Zheng, Y.; Newman, C. E.; Quin, J.; Dolz, F.; Kastler, M.; Facchetti, A. *Nature* **2009**, *457*, 679. (b) Tang, M. L.; Mannsfeld, S. C. B.; Sun, Y.-S.; Becerril, H. A.; Bao, Z. *J. Am. Chem. Soc.* **2009**, *131*, 882. (c) Xia, Y.; Cho, J.; Paulsen, B.; Frisbie, C. D.; Renn, M. *J. Appl. Phys. Lett.* **2009**, *94*, 013304-1. (d) Molinari, A. S.; Alves, H.; Chen, Z.; Facchetti, A.; Morpurgo, A. F. *J. Am. Chem. Soc.* **2009**, *131*, 2462. (e) Allard, S.; Forster, M.; Souharce, B.; Thiem, H.; Sherf, U. *Angew. Chem., Int. Ed.* **2008**, *47*, 4070. (f) Lu, G.; Usta, H.; Risko, C.; Wang, L.; Facchetti, A.; Ratner, M. A.; Marks, T. J. *J. Am. Chem. Soc.* **2008**, *130*, 7670. (g) Letizia, J. A.; Salata, M. R.; Tribout, C. M.; Facchetti, A.; Ratner, M. A.; Marks, T. J. *J. Am. Chem. Soc.* **2008**, *130*, 9679. (h) Tang, M. L.; Reichardt, A. D.; Miyaki, N.; Stoltenberg, R. M.; Bao, Z. *J. Am. Chem. Soc.* **2008**, *130*, 6064. (i) Brusso, J. L.; Hirst, O. D.; Dadvand, A.; Ganesan, S.; Cicoira, F.; Robertson, C. M.; Oakley, R. T.; Rosei, F.; Perepichka, D. F. *Chem. Mater.* **2008**, *20*, 2484. (j) Okamoto, H.; Kawasaki, N.; Kaji, Y.; Kubozono, Y.; Fujiwara, A.; Yamaji, M. *J. Am. Chem. Soc.* **2008**, *130*, 10470. (k) Jones, B. A.; Facchetti, A.; Wasielewski, M. R.; Marks, T. J. *J. Am. Chem. Soc.* **2007**, *129*, 15259. (l) Facchetti, A. *Mater. Today* **2007**, *10*, 28. (m) Murphy, A. R.; Frechet, J. M. J. *Chem. Rev.* **2007**, *107*, 1066. (n) Zaunseil, J.; Sirringhaus, H. *Chem. Rev.* **2007**, *107*, 1296.

these materials, members of the (poly)arylacetylene family are particularly attractive,⁵ because of their flexible molecular orbital energetics, known⁶ to be tunable *via* appropriate skeletal functionalization. Moreover, the availability of efficient synthetic protocols⁷ allows the effective π -conjugation length of these shape-persistent rod-like structures to be easily varied by controlling the number of arylacetylene repeat units. Note also that alkyne linkages are more accommodating than alkenes to steric and conformational constraints due to the *quasi*-cylindrical electronic symmetry.⁸

The results of Roy et al.^{5d} on OFET-determined charge transport indicate that vacuum-deposited thin films of arylacetylene oligomers can exhibit field-effect hole mobilities (μ) as high as $0.3 \text{ cm}^2 \text{ V}^{-1} \text{ s}^{-1}$ and current on-off ratios ($I_{\text{on}}/I_{\text{off}}$) $\approx 10^5$. Yasuda et al.^{5c} also reported high-performance OFETs using vacuum-deposited diethynyl-naphthalene derivatives, and a maximum field-effect hole mobility of $0.12 \text{ cm}^2 \text{ V}^{-1} \text{ s}^{-1}$ and $I_{\text{on}}/I_{\text{off}} \approx 10^5$ were reported (**BH-202**). Very recently, Meng et al.^{5a} reported that films of soluble conjugated thiophene-ethynylphenylene semiconductors exhibit charge carrier mobilities as high as $0.084 \text{ cm}^2 \text{ V}^{-1} \text{ s}^{-1}$ with $I_{\text{on}}/I_{\text{off}} = 10^5$. A promising approach to combining good transistor characteristics and high solar energy conversion efficiencies has been reported by Baek

Chart 1. Representative Semiconducting (Poly)arylacetylenes



et al.⁹ Here it was shown that, for solution-processable metalated polyarylacetylenes, field-effect mobilities and $I_{\text{on}}/I_{\text{off}}$ ratios approach $0.01 \text{ cm}^2 \text{ V}^{-1} \text{ s}^{-1}$ and 10^4 , respectively, and solar cell power conversion efficiencies (PCEs) reach 3.73% (**P4**). Spin-coated metal-containing polyarylacetylenes have also been successfully used by other groups as active layers in bulk heterojunction solar cells.¹⁰ An important result of Cremer et al.¹¹ is the finding that poly(ethynylene-bithienylene) (**PEBT**)/PCBM devices exhibit significantly greater V_{oc} values ($\sim 1.0 \text{ V}$) than PH3T/PCBM solar cells ($V_{\text{oc}} \approx 0.62 \text{ V}$),¹² highlighting the attraction of incorporating electron-withdrawing ethynylene units into polymer backbones (Chart 1).

Taking all of these results into account, the development of new arylacetylene structures should afford interesting and instructive new hole-transporting materials for OFETs as well as for OPVs. Furthermore, very few solution-processable arylacetylenes suitable for OPVs are known,¹³ and those which have been reported generally exhibit modest power conversion efficiencies. Small-molecule donor materials offer attractions over polymeric materials in terms of ease of synthesis and purification, which greatly improves fabrication reproducibility, as well as exhibiting a greater tendency to self-assemble into ordered domains, affording high charge carrier mobilities. Most important, small molecules do not suffer from batch-to-batch property variations or end-group contamination as do their polymeric counterparts. Finally, parameters such as polydispersity and regioregularity are not an issue.

- (3) (a) Nelson, J.; Kwiatkowski, J. J.; Kirkpatrick, J.; Frost, J. M. *Acc. Chem. Res.* **2009**, *42*, 1768. (b) Cheng, Y.-J.; Yang, S.-H.; Hsu, C.-S. *Chem. Rev.* **2009**, *109*, 5868. (c) Heremans, P.; Cheyons, D.; Rand, B. P. *Acc. Chem. Res.* **2009**, *42*, 1740. (d) Denler, G.; Sharber, M. C.; Brabec, C. *Adv. Mater.* **2009**, *21*, 1323. (e) Liang, Y.; Feng, D.; Guo, J.; Szarko, J. M.; Ray, C.; Chen, L. X.; Yu, L. *Macromolecules* **2009**, *42*, 1091. (f) Palilis, L. C.; Lane, P.; Kushto, G. P.; Purushothaman, B.; Anthony, J.; Kafafi, Z. H. *Org. Electron.* **2008**, *9*, 747. (g) Ooi, Z. E.; Tam, T. L.; Shin, R. Y. C.; Chen, Z. K.; Kietzke, T.; Sellinger, A.; Baumgarten, M.; Müllen, K.; deMello, J. J. *Mater. Chem.* **2008**, *18*, 4619. (h) Thompson, B. C.; Fréchet, J. M. *Angew. Chem., Int. Ed.* **2008**, *47*, 58. (i) Günes, S.; Neugebauer, H.; Sariciftci, N. S. *Chem. Rev.* **2007**, *107*, 1324. (j) Rand, B. P.; Genoe, J.; Heremans, P.; Poortmans, J. *Prog. Photovolt: Res. Appl.* **2007**, *15*, 659.
- (4) (a) Wei, S. K. H.; Chen, S. H.; Dolgaleva, K.; Lukishova, S.; Boyd, R. W. *Appl. Phys. Lett.* **2009**, *94*, 041111/1. (b) Amarasinghe, D.; Ruseckas, A.; Vasdekis, A. E.; Turnbull, G. A.; Samuel, I. D. W. *Appl. Phys. Lett.* **2008**, *92*, 083305/1. (c) Holmes, R. J.; Forrest, S. R. *Org. Electron.* **2007**, *8*, 77. (d) Yamashita, K.; Arimatsu, A.; Takeuchi, N.; Takayama, M.; Oe, K.; Yanagi, H. *Appl. Phys. Lett.* **2008**, *93*, 233303/1. (e) Zavelani-Rossi, M.; Lanzani, G.; De Silvestri, S.; Anni, M.; Gigli, G.; Cingolani, R.; Barbarella, G.; Favaretto, L. *Appl. Phys. Lett.* **2001**, *79*, 4082.
- (5) (a) Meng, Q.; Gao, J.; Li, R.; Jiang, L.; Wang, C.; Zhao, H.; Liu, C.; Li, H.; Hu, W. *J. Mater. Chem.* **2009**, *19*, 1477. (b) Huang, X.; Zhu, C.; Zhang, S.; Li, W.; Guo, Y.; Zhan, X.; Liu, Y.; Bo, Z. *Macromolecules* **2008**, *41*, 6895. (c) Yasuda, T.; Kashiwagi, K.; Morizawa, Y.; Tsutsui, T. *J. Phys. D: Appl. Phys.* **2007**, *40*, 4471. (d) Roy, V. A. L.; Zhi, Y.-G.; Xu, Z.-X.; Yu, S.-C.; Chan, P. W. H.; Che, C.-M. *Adv. Mater.* **2005**, *17*, 1258. (e) Cornil, J.; Karzazi, Y.; Bredas, J. L. *J. Am. Chem. Soc.* **2002**, *124*, 3516. (f) McQuade, D. T.; Pullen, A. E.; Swager, T. M. *Chem. Rev.* **2000**, *100*, 2537. (g) Tour, J. M. *Acc. Chem. Res.* **2000**, *33*, 791. (h) Martin, R. E.; Diederich, F. *Angew. Chem., Int. Ed.* **1999**, *38*, 1350. (i) McDonagh, A. M.; Humphrey, M. G.; Samoc, M.; Luther-Davies, B.; Houbrechts, S.; Wada, T.; Sasabe, H.; Persoons, A. *J. Am. Chem. Soc.* **1999**, *121*, 1405. (j) Kraft, A.; Grimsdale, A. C.; Holmes, A. B. *Angew. Chem., Int. Ed.* **1998**, *37*, 402.
- (6) (a) Li, C.; Li, Y. *Macromol. Chem. Phys.* **2008**, *209*, 1541. (b) Bunz, U. H. F. *Chem. Rev.* **2000**, *100*, 1605.
- (7) (a) Zhang, W.; Kraft, S.; Moore, J. S. *J. Am. Chem. Soc.* **2004**, *126*, 329. (b) Siemsen, P.; Livingstone, R. C.; Diederich, F. *Angew. Chem., Int. Ed.* **2000**, *39*, 2632. (c) Schrock, R. R. *Polyhedron* **1995**, *14*, 3177. (d) Sonogashira, K. *Metal Catalyzed Cross-Coupling Reactions*; Wiley-VCH: Weinheim, 1998. (e) Weiss, K.; Michel, A.; Auth, E.-M.; Bunz, E. H. F.; Mangel, T.; Mullen, K. *Angew. Chem., Int. Ed. Engl.* **1997**, *36*, 506.
- (8) Diederich, F.; Stang, P. J.; Tykwinski, R. R., Eds. *Acetylene Chemistry: Chemistry, Biology and Materials Science*; Wiley-VCH: Weinheim, 2005.

- (9) Baek, N. S.; Hau, S. K.; Yip, H.-L.; Acton, O.; Chen, K.-S.; Jen, A. K.-Y. *Chem. Mater.* **2008**, *20*, 5734.
- (10) (a) Mei, J.; Ogawa, K.; Kim, Y.-G.; Heston, N. C.; Arenas, D. J.; Nasrollahi, Z.; McCarley, T. D.; Tanner, D. B.; Reynolds, J. R.; Schanze, K. S. *ACS Appl. Mater. Interfaces* **2009**, *1*, 150. (b) Wu, P.-T.; Bull, T.; Kim, F. S.; Luscombe, C. K.; Jenekhe, S. A. *Macromolecules* **2009**, *42*, 671. (c) Liu, L.; Ho, C.-K.; Wong, W.-Y.; Cheung, K.-Y.; Fung, M.-K.; Lam, W.-T.; Djuricic, A.; Chan, W.-K. *Adv. Funct. Mater.* **2008**, *18*, 2824. (d) Wong, W.-Y.; Wang, X.-Z.; He, Z.; Djuricic, A. B.; Yip, C.-T.; Cheung, K.-Y.; Wang, H.; Mak, C. S. K.; Chan, W. K. *Nat. Mater.* **2007**, *6*, 521.
- (11) Cremer, J.; Bauerle, P.; Wienk, M. M.; Janssen, R. A. J. *Chem. Mater.* **2006**, *18*, 5832.
- (12) (a) Kim, Y.; Cook, S.; Tuladhar, S. M.; Choulis, S. A.; Nelson, J.; Durrant, J. R.; Bradley, D. D. C.; Giles, M.; McCulloch, I.; Ha, C. S.; Ree, M. *Nat. Mater.* **2006**, *5*, 197. (b) Li, G.; Shrotriya, V.; Huang, J.; Yao, Y.; Moriarty, T.; Emery, K.; Yang, Y. *Nat. Mater.* **2005**, *4*, 864. (c) Ma, W.; Yang, C.; Gong, X.; Lee, K.; Heeger, A. J. *Adv. Funct. Mater.* **2005**, *15*, 1617.
- (13) (a) Fernandez, G.; Sanchez, L.; Veldman, D.; Wienk, M. M.; Atienza, C.; Guldi, D. M.; Janssen, R. A. J.; Martin, N. *J. Org. Chem.* **2008**, *73*, 3189. (b) Valentini, L.; Marrocchi, A.; Seri, M.; Mengoni, F.; Meloni, F.; Taticchi, A.; Kenny, J. M. *Thin Solid Films* **2008**, *516*, 7193. (c) Guo, F.; Ogawa, K.; Kim, Y.-G.; Danilov, E. O.; Castellano, F. N.; Reynolds, J. R.; Schanze, K. S. *Phys. Chem. Chem. Phys.* **2007**, *9*, 2724. (d) Atienza, C. M.; Fernandez, G.; Sanchez, L.; Martin, N.; Sa Dantas, I.; Wienk, M. M.; Janssen, R. A. J.; Raman, G. M. A.; Guldi, D. M. *Chem. Commun.* **2006**, 514. (e) Nierengarten, J.-F.; Gu, T.; Aernouts, T.; Geens, W.; Poortmans, J.; Hadziioannou, G.; Tsamouras, D. *Appl. Phys. A: Mater. Sci. Process.* **2004**, *79*, 47.

Chart 2. Structures of Anthracene-Based Derivatives 1–4

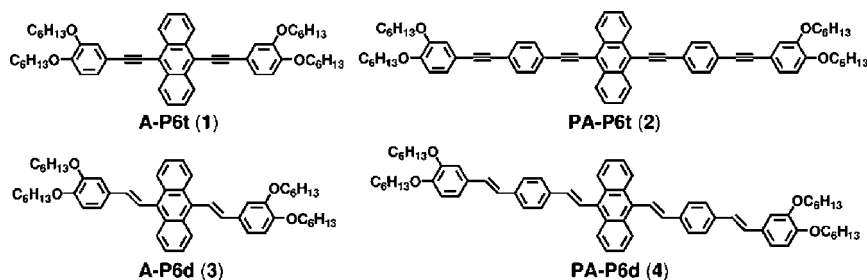
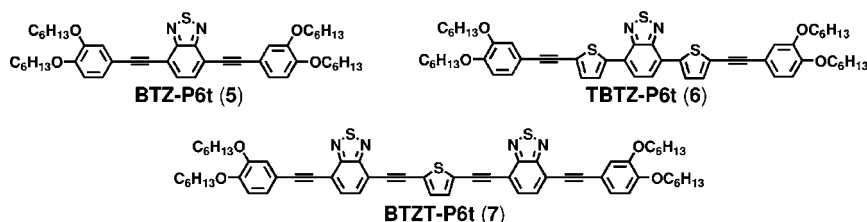


Chart 3. Structures of 2,1,3-Benzothiadiazole-Based Derivatives 5–7



In a recent communication¹⁴ we briefly described the synthesis of compounds **A-P6t** and **PA-P6t** (Chart 2) and their implementation in bulk heterojunction (BHJ) solar cells, yielding PCEs up to $\sim 1.2\%$. We also showed recently¹⁵ that OFETs based on extended arylacetylenes **PA-P6t** and **TBTZ-P6t** (Charts 2 and 3) exhibit substantial hole mobilities, approaching $0.1 \text{ cm}^2 \text{ V}^{-1} \text{ s}^{-1}$ with on/off ratios up to $\sim 10^7$.

In this contribution, we report the synthesis and characterization of previously unknown members of this extended arylacetylene series, to further explore and elucidate architecture-electronic structure relationships in this semiconductor class. Solution-processable OFETs and BHJ photovoltaic cells (Figure 1) are fabricated and optimized for compounds 1–7, and their device responses characterized. The design strategy in the present semiconductor family aims at achieving high solubility in common organic solvents, efficient hole transport (required for optimum OFET and OPV response), and broad NIR-shifted optical absorption, to capture maximum solar light. Enhanced solubility is achieved by introducing alkoxy chains onto the delocalized core peripheries. Additionally, this approach promotes molecular self-organization in the solid state.¹⁶

Note that anthracene-based compounds **A-P6t** (1), **PA-P6t** (2), **A-P6d** (3), **PA-P6d** (4) are designed bearing in mind that *n*-acenes exhibit some of the highest known OFET mobilities ($\mu = 5.5 \text{ cm}^2 \text{ V}^{-1} \text{ s}^{-1}$ for pentacene).^{17–19} However, useful chemical modification of large acenes is challenging because of the generally low solubility. Therefore, we employed anthracene,²⁰ which is more readily derivatized to afford greater solubility and chemical stability.²¹ It is known that anthracene oligomer-based OFETs can exhibit high hole mobilities,^{21c} suggesting that anthracene π -extension by interposed arylene fragments can afford efficient charge transporting structures.

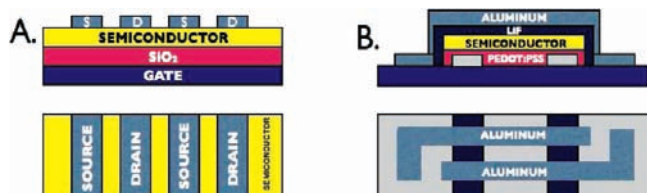


Figure 1. Schematic representation of (A) field-effect transistor and (B) bulk heterojunction solar cell structures employed in this study.

Additionally, high field-effect mobilities are relevant for solar cell applications since this can enhance exciton diffusion lengths, remove photogenerated electron–hole pairs before recombination, and efficiently convey carriers to the electrodes for collection.^{12b,22} Furthermore, unsubstituted acenes typically pack in a herringbone motif^{23,24a} whereas appropriate arene substitution may promote face-to-face π -stacking.^{24–26} In several cases,

- (14) Marrocchi, A.; Silvestri, F.; Seri, M.; Facchetti, A.; Taticchi, A.; Marks, T. J. *Chem. Commun.* **2009**, 1380.
- (15) Marrocchi, A.; Seri, M.; Kim, C.; Facchetti, A.; Taticchi, A.; Marks, T. J. *Chem. Mater.* **2009**, *21*, 2592.
- (16) (a) Sung, A.; Ling, M.; Tang, M. L.; Bao, Z.; Locklin, J. *Chem. Mater.* **2007**, *19*, 2342. (b) Wurthner, F.; Schmidt, R. *Chem. Phys. Chem.* **2006**, *7*, 793. (c) Locklin, J.; Roberts, M. E.; Mannsfeld, S. C. B.; Bao, Z. *Polym. Rev.* **2006**, *46*, 79.
- (17) Lee, S.; Koo, B.; Shin, J.; Lee, E.; Park, H.; Kim, H. *Appl. Phys. Lett.* **2006**, *88*, 162109.
- (18) (a) Okamoto, T.; Senatore, M. L.; Ling, M.-M.; Mallik, A. B.; Tang, M. L.; Bao, Z. *Adv. Mater.* **2007**, *19*, 3381. (b) Payne, M. M.; Parkin, S. R.; Anthony, J. E.; Kuo, C.-C.; Jackson, T. N. *J. Am. Chem. Soc.* **2005**, *127*, 4986. (c) Meng, H.; Bendikov, M.; Mitchell, G.; Hegelson, R.; Wudd, F.; Bao, Z.; Siegrist, T.; Klock, C.; Chen, C. H. *Adv. Mater.* **2003**, *15*, 1090.
- (19) (a) Ruiz Delgado, M. C.; Pigg, K. R.; da Silva Filho, D. A.; Gruhn, N. E.; Sakamoto, Y.; Suzuki, T.; Osuna, R. M.; Casado, J.; Hernandez, V.; Lopez Navarrete, J. T.; Martinelli, N. G.; Cornil, J.; Sanchez-Carrera, R. S.; Coropceanu, V.; Bredas, J. L. *J. Am. Chem. Soc.* **2009**, *131*, 1502. (b) Sakamoto, Y.; Suzuki, T.; Kobayashi, M.; Gao, Y.; Fukai, Y.; Inoue, Y.; Sato, F.; Tokito, S. *J. Am. Chem. Soc.* **2004**, *126*, 8138.
- (20) Pope, M.; Swenberg, C. E. *Electronic Processes in Organic Crystals and Polymers*; Oxford University Press: New York, 1999.
- (21) (a) Anthony, J. E. *Chem. Rev.* **2006**, *106*, 5028. (b) Meng, H.; Sun, F.; Goldfinger, A. B.; Jaycox, G. D.; Li, Z.; Marshall, J.; Blackman, G. S. *J. Am. Chem. Soc.* **2005**, *127*, 2406. (c) Ito, K.; Suzuki, T.; Sakamoto, Y.; Kubota, D.; Inoue, Y.; Sato, F.; Tokito, S. *Angew. Chem., Int. Ed.* **2003**, *42*, 1159. (d) Clar, E. *Polycyclic Hydrocarbons*, Vol. 1; Academic Press: New York, 1964.
- (22) Brabec, C. J. *Sol. Energy Mater. Sol. Cells* **2004**, *83*, 273.
- (23) (a) Fritz, S. E.; Martin, S. M.; Frisbie, C. D.; Ward, M. D.; Toney, M. F. *J. Am. Chem. Soc.* **2004**, *126*, 4084. (b) Cornil, J.; Calbert, J. P.; Bredas, J.-L. *J. Am. Chem. Soc.* **2001**, *123*, 1250.
- (24) (a) Wang, C.; Liu, Y.; Ji, Z.; Wang, E.; Li, R.; Jiang, H.; Tang, Q.; Li, H.; Hu, W. *Chem. Mater.* **2009**, *21*, 2840. (b) Schmidt, R.; Gottling, S.; Leusser, D.; Stalke, D.; Krause, A.-M.; Wurthner, F. *J. Mater. Chem.* **2006**, *16*, 3708. (c) Sarma, J. A. R. P.; Desiraju, G. R. *Acc. Chem. Res.* **1986**, *19*, 222.
- (25) (a) Sasaki, H.; Wakayama, Y.; Chikyow, T.; Barrena, E.; Dosch, H.; Kobayashi, K. *Appl. Phys. Lett.* **2006**, *88*, 081907. (b) Kobayashi, K.; Masu, H.; Shuto, A.; Yamaguchi, K. *Chem. Mater.* **2005**, *17*, 6666.

e.g., going from pentacene and oligothiophenes (herringbone) to TIPS pentacene or mixed fluoroarene-thiophene oligomers (cofacial π -stacking), respectively, this approach resulted in enhanced carrier mobilities.^{2m,21a}

These considerations suggest the potential of derivatives **1–4** for a cofacial π -stacking and for elucidating^{14,27} the effects of replacing olefinic with acetylenic linkers in organic semiconductors. Additionally, we report here 2,1,3-benzothiadiazole (BTZ)-containing arylacetylene derivatives **BTZ-P6t (5)**, **TBTZ-P6t (6)**, and **BTZT-P6t (7)**. It is known that 2,1,3-benzothiadiazoles have high electron affinities and are amenable to facile ring modification.²⁸ Moreover, BTZ-containing compounds generally afford well-organized crystal structures due to their significant polarizability, leading to intermolecular interactions such as heteroatom...heteroatom contact and π - π interactions.²⁹ For these reasons, we synthesized new arylacetylene **BTZ-P6t** as an analogue of compound **A-P6t** in which a BTZ unit replaces the anthracene core. However, in compound **TBTZ-P6t** the benzothiadiazole core is substituted with a donor-acceptor-donor (D-A-D) motif by introducing thienyl groups on either side of a 2,1,3-benzothiadiazole unit.¹⁵ It is well-established that intramolecular charge transfer from electron-rich to electron-deficient moieties lowers the band gap,³⁰ desirable for OPV light absorption at longer wavelengths.^{9,31} It is also known³² that such D-A-D motifs enhance molecular core coplanarity due to intramolecular charge transfer, which is further supported by computation.³³ In designing compound **TBTZ-P6t**, we also recognized the possibility of strong dipole-dipole-induced intermolecular interactions.^{28a,34,35} Finally, novel compound **TBTZ-P6t** was created with an extended conjugation length by introducing a donor-acetylene-acceptor unit.^{28c,36} This offers

the potential for enhanced intramolecular charge transfer character, thereby influencing solid state packing and carrier transport.

OFETs based on arylacetylenes **1–7** are optimized here in terms of solvent selection and film processing methodology. It will be seen that materials having hole mobilities approaching $0.1 \text{ cm}^2 \text{ V}^{-1} \text{ s}^{-1}$ with $I_{\text{on}}/I_{\text{off}} > 10^6$ can be obtained with devices fabricated by simple spin-coating techniques. Solution-processable BHJ solar cells are also fabricated and optimized, and their device responses analyzed in terms of the interplay between molecular electronic structure and film microstructural/morphological characteristics. Furthermore, C \equiv C triple bonds are shown here to be effective C=C replacements and to afford both high OPV open circuit voltage (V_{oc}) and good short circuit current (J_{sc}) metrics, as well as power conversion efficiencies of $\sim 1.3\%$. Finally, this study reveals close, instructive correlations between semiconductor FET mobility and BHJ OPV performance.

Experimental Section

Materials and Methods. All reagents were purchased from commercial sources and used without further purification unless otherwise noted. PCBM was purchased from American Dye Source, Inc. (ADS) and was further purified by several cycles of sonication in toluene followed by filtration and then sonication in pentane, followed by centrifugation. Anhydrous THF was distilled from Na/benzophenone, and toluene was distilled from LiAlH₄. Petroleum ether was used as the 40–60 °C boiling fraction. Solution optical spectra were recorded on a Cary Model 1 UV-vis spectrophotometer. NMR spectra were recorded on a Varian Associates VXR-400 multinuclear spectrometer (internal Me₄Si). Elemental analyses were performed on a Fisons EA 1108 instrument.

Synthesis of 4,7-Bis-([m,p-bis(hexyloxy)phenyl]ethynyl)-2,1,3-benzothiadiazole (BTZ-P6t, 5). Dry toluene (6 mL), 4,7-dibromo-2,1,3-benzothiadiazole **9** (0.15 g, 0.51 mmol), CuI (0.004 g, 0.02 mmol), Pd(PPh₃)₄ (0.025 g, 0.02 mmol), and diisopropylamine (3 mL) were placed in a flask and degassed with argon at 0 °C. Next, 3,4-(bis(hexyloxy)-ethynyl)benzene **8** (0.33 g, 1.1 mmol) was added and the mixture was kept at 50 °C for 18 h. The solvent was then evaporated to dryness, and the crude product was purified by column chromatography (silica gel, petroleum ether/dichloromethane 3:2) to afford **BTZ-P6t** (80% yield, yellow crystals); mp 139–140 °C (ethyl acetate); ¹H NMR (CDCl₃): δ 0.85 (m, 12 H), 1.26–1.44 (m, 24H), 1.77 (m, 8H); 4.02 (m, 8H), 7.20 (m, 4H), 7.10 (s, 2H), 7.68 (s, 2H); ¹³C NMR (CDCl₃): δ 154.4, 150.3, 148.7, 132.2, 125.6, 117.1, 116.6, 114.4, 112.9, 98.1, 84.0, 69.3, 69.1, 31.6, 29.2, 29.1, 25.7, 22.6, 14.1; UV-vis (CHCl₃) [λ_{max} nm (log ϵ)] 311 (4.6), 447 (4.4). Anal. Calcd for C₄₆H₆₀N₂O₄S: C, 74.96; H, 8.21; N, 3.80; S, 4.35. Found: C, 75.33; H, 8.20; N, 3.77; S, 4.32%.

Synthesis of 4-([m,p-Bis(hexyloxy)phenyl]ethynyl)-7-bromo-2,1,3-benzothiadiazole (10). 4,7-Dibromo-2,1,3-benzothiadiazole (**9**) was coupled with 3,4-(bis(hexyloxy)-ethynyl)benzene **8** (1:0.5 ratio), following the above procedure. Reaction time: 10 h. The crude product was purified by column chromatography (silica gel, hexane/chloroform 7:3). Yield: 51% (yellow solid); mp: 94–95 °C (ethyl

- (26) Sun, Y.-Q.; Tsang, C.-K.; Xu, Z.; Huang, G.; He, J.; Zhou, X.-P.; Zeller, M.; Hunter, A. D. *Cry. Growth Des.* **2008**, *8*, 1468.
 (27) (a) Egbe, D. A. M.; Wild, A.; Bircner, E.; Grummt, U.-W.; Schubert, U. S. *Macromol. Symp.* **2008**, *25*. (b) Egbe, D. A. M.; Nguyen, L. H.; Mühlbacher, D.; Hoppe, H.; Schmidke, K.; Sariciftci, N. S. *Thin Solid Films* **2006**, *511–512*, 486. (c) Egbe, D. A. M.; Nguyen, L. H.; Carbonnier, B.; Mühlbacher, D.; Sariciftci, N. S. *Polymers* **2005**, *46*, 9585. (d) Hoppe, H.; Egbe, D. A. M.; Mühlbacher, D.; Sariciftci, N. S. *J. Mater. Chem.* **2004**, *14*, 3462.
 (28) (a) Sonar, P.; Singh, S. P.; Sudhakar, S.; Dodabalapur, A.; Sellinger, A. *Chem. Mater.* **2008**, *20*, 3184. (b) Kono, T.; Kumaki, D.; Nishida, J.-I.; Sakanoue, T.; Kakita, M.; Tada, H.; Tokito, S.; Yamashita, Y. *Chem. Mater.* **2007**, *19*, 1218–1220. (c) Akhtaruzzaman, M.; Tomura, M.; Nishida, J.; Yamashita, Y. *J. Org. Chem.* **2004**, *69*, 2953.
 (29) (a) Yamashita, Y.; Ono, K.; Tomura, M.; Imaeda, K. *Chem. Commun.* **1997**, 1851. (b) Yamashita, Y.; Tomura, M.; Imaeda, K. *Chem. Commun.* **1996**, 2021. (c) Ono, K.; Tanaka, S.; Yamashita, Y. *Angew. Chem., Int. Ed.* **1994**, *33*, 1977. (d) Suzuki, T.; Fujii, H.; Yamashita, Y.; Kabuto, C.; Tanaka, S.; Harasawa, M.; Mukai, T.; Miyashi, T. *J. Am. Chem. Soc.* **1992**, *114*, 3034.
 (30) (a) Park, Y. S.; Kim, D.; Hoosung, L.; Moon, B. *Org. Lett.* **2006**, *8*, 4702. (b) Jaykannan, M.; Van Hal, P. A.; Janssen, R. A. *J. Polym. Sci., Part A: Polym. Chem.* **2001**, *40*, 251. (c) van Müllekom, H. A. M.; Venkemans, J. A. J. M.; Meijer, E. W. *Chem.—Eur. J.* **1998**, *4*, 1235.
 (31) (a) Hou, J.; Chen, H.-Y.; Zhang, S.; Li, G.; Yang, Y. *J. Am. Chem. Soc.* **2008**, *130*, 16144. (b) Zaumseil, J.; Sirringhaus, H. *Chem. Rev.* **2007**, *107*, 296. (c) Blouin, N.; Michaud, A.; Leclerc, M. *Adv. Mater.* **2007**, *19*, 2295. (d) Peet, J.; Kim, J. Y.; Coates, N. E.; Ma, W. L.; Moses, D.; Heeger, A. J.; Bazan, J. C. *Nat. Mater.* **2007**, *6*, 497. (e) Mühlbacher, D.; Scharber, M.; Morana, M.; Zhu, Z.; Waller, D.; Gaudiana, R.; Brabec, C. J. *Adv. Mater.* **2006**, *18*, 2884.
 (32) Akhtaruzzaman, M.; Kamata, N.; Nishida, J.-i.; Ando, S.; Tada, H.; Tomura, M.; Yamashita, Y. *Chem. Commun.* **2005**, 3183.
 (33) Ozen, A. S.; Atilgan, C.; Sonmez, G. *J. Phys. Chem. C* **2007**, *111*, 16362.

- (34) (a) Melucci, M.; Favaretto, L.; Bettini, C.; Gazzano, M.; Camaioni, M.; Maccagnani, P.; Ostoja, P.; Monari, M.; Barbarella, G. *Chem.—Eur. J.* **2007**, *13*, 10046. (b) Kono, T.; Kumaki, D.; Nishida, J.-i.; Sakanoue, T.; Kakita, M.; Tada, H.; Tokito, S.; Yamashita, Y. *Chem. Mater.* **2007**, *19*, 1218.
 (35) Neto, B. A. D.; Lopes, A. S. A.; Ebeling, G.; Goncalves, R. S.; Costa, V. E. U.; Quina, F. H.; Dupont, J. *Tetrahedron* **2005**, *46*, 10975.
 (36) (a) Lehmann, M.; Seltmann, J.; Auer, A. A.; Prochnow, E.; Benedikt, U. *J. Mater. Chem.* **2009**, *19*, 1978. (b) Yasuda, T.; Imase, T.; Nakamura, Y.; Yamamoto, T. *Macromolecules* **2005**, *38*, 4687. (c) Akhtaruzzaman, M.; Tomura, M.; Nishida, J.-i.; Yamashita, Y. *J. Org. Chem.* **2004**, *69*, 2953. (d) Kato, S.-i.; Matsumoto, T.; Ishi-i, T.; Thiemann, T.; Shigeiva, M.; Gorohmaru, H.; Maeda, S.; Yamashita, Y.; Mataka, S. *Chem. Commun.* **2004**, 2342.

acetate); ^1H NMR (CDCl_3): δ 0.86 (m, 6H), 1.25–1.51 (m, 12H), 1.81 (m, 4H), 3.96 (m, 4H), 6.81 (d, 1H, $J = 8.0$ Hz), 7.09 (d, 1H, $J = 3.0$ Hz), 7.16–7.20 (m, 1H), 7.61 (d, 1H, $J = 8.0$ Hz), 7.80 (d, 1H, $J = 8.0$ Hz); ^{13}C NMR (CDCl_3): δ 154.1, 153.0, 150.4, 148.7, 132.4, 132.0, 125.6, 116.7, 114.2, 114.0, 113.0, 97.6, 83.2, 69.3, 69.0, 31.5, 29.1, 25.6, 22.6, 14.0. Anal. Calcd for $\text{C}_{26}\text{H}_{31}\text{BrN}_2\text{O}_2\text{S}$: C, 60.58; H, 6.06; N, 5.43; S, 6.22. Found: C, 60.91; H, 6.05; N, 5.46; S, 6.18%.

Synthesis of 4-([*m,p*-Bis(hexyloxy)phenyl]ethynyl)-7-[(trimethylsilyl)ethynyl]-2,1,3-benzothiadiazole (11). This compound was prepared by coupling of **10** with trimethylsilylacetylene (1:4 molar ratio), following the above procedure. Reaction time: 10 h. Reaction temperature: 25 °C. The crude product was purified by column chromatography (silica gel, hexane/chloroform 65:35). Yield: 93% (yellow solid); mp: 53–54 °C (ethyl acetate); ^1H NMR (CDCl_3): δ 0.28 (s, 9H), 0.86 (m, 6H), 1.26–1.51 (m, 12H), 1.86–1.75 (m, 4H), 3.98 (m, 4H), 6.81 (d, 1H, $J = 8.0$ Hz), 7.11–7.18 (m, 2H), 7.70 (m, 2H); ^{13}C NMR (CDCl_3): δ 154.3, 150.4, 148.7, 133.4, 131.8, 125.6, 117.9, 116.7, 116.3, 114.3, 113.0, 103.2, 100.1, 98.4, 83.9, 69.3, 69.0, 31.5, 29.2, 29.1, 25.6, 22.6, 14.0, –0.1. Anal. Calcd for $\text{C}_{31}\text{H}_{41}\text{N}_2\text{O}_2\text{SSi}$: C, 69.88; H, 7.57; N, 5.26; S, 6.02. Found: C, 70.23; H, 7.56; N, 5.29; S, 6.05%.

Synthesis of 4-([*m,p*-Bis(hexyloxy)phenyl]ethynyl)-7-ethynyl-2,1,3-benzothiadiazole (12). To a solution of **11** (0.47 g, 0.88 mmol) in dry THF (15 mL) was added tetrabutylammonium fluoride (1.06 mL, 1.06 mmol). The reaction mixture was kept under nitrogen and magnetically stirred at 25 °C for 1 h. The solvent was then removed in *vacuo*. The residue was purified by column chromatography (silica gel, hexane/dichloromethane 3:1) to obtain compound **12** (88% yield) as a yellow solid; mp: 64–65 °C (ethyl acetate); ^1H NMR (CDCl_3): δ 0.86 (m, 6H), 1.26–1.51 (m, 12H), 1.75–1.86 (m, 4H), 3.26 (s, 1H), 3.98 (m, 4H), 6.81 (d, 1H, $J = 8.0$ Hz), 7.11–7.18 (m, 2H), 7.72 (m, 2H); ^{13}C NMR (CDCl_3): δ 148.7, 144.3, 142.6, 133.6, 131.7, 125.7, 116.7, 114.2, 113.0, 98.5, 97.9, 84.7, 69.3, 69.1, 31.6, 29.2, 25.7, 22.6, 14.0. Anal. Calcd for $\text{C}_{28}\text{H}_{32}\text{N}_2\text{O}_2\text{S}$: C, 73.01; H, 7.00; N, 6.08; S, 6.96. Found: C, 73.40; H, 7.01; N, 6.11; S, 6.99%.

Synthesis of 7,7'-([*m,p*-Bis(hexyloxy)phenyl]ethynyl)-2,1,3-benzothiadiazol-4,4'-ethynyl)-2,5-thiophene (BTZT-P6t, **7).** This compound was prepared by coupling **12** with 2,5-dibromothiophene (2.2:1 molar ratio) following the procedure described for **BTZ-P6t** (**5**). Reaction temperature: 55 °C. The crude product was purified by column chromatography (silica gel, petroleum ether/dichloromethane 1:1). Yield: 89% (orange solid); mp 188–189 °C (ethyl acetate); ^1H NMR (CDCl_3): δ 0.86 (m, 12H), 1.24–1.49 (m, 24 H), 1.75–1.83 (m, 8H), 3.97 (m, 8H), 6.81 (d, 2H, $J = 8.0$ Hz), 7.10 (m, 2H), 7.18–7.20 (m, 2H), 7.32 (s, 2H), 7.70–7.80 (m, 4H); ^{13}C NMR (CDCl_3): δ 154.4, 154.1, 150.6, 148.8, 133.2, 132.6, 131.9, 125.8, 125.0, 118.1, 116.8, 115.8, 114.4, 113.1, 98.8, 90.7, 89.8, 84.0, 69.3, 69.1, 31.6, 29.2, 29.1, 25.6, 22.6, 14.0; UV–vis (CHCl_3) [λ_{max} nm (log ϵ)] 319 (4.8), 328 (4.9), 472 (5.0). Anal. Calcd for $\text{C}_{60}\text{H}_{64}\text{N}_4\text{O}_4\text{S}_3$: C, 71.97; H, 6.44; N, 5.60; S, 9.61. Found: C, 72.01; H, 6.43; N, 5.63; S, 9.55%.

Electrochemistry. Cyclic voltammetry measurements were performed on a C3 Cell Stand electrochemical station equipped with BAS Epsilon software (Bioanalytical Systems, Inc., Lafayette, IN) with a 0.1 M tetrabutylammonium hexafluorophosphate ($\text{Bu}_4\text{N}^+\text{PF}_6^-$) electrolyte in dry CH_2Cl_2 . Platinum wire electrodes were used as both working and counter electrodes, and a Ag wire was used as the pseudoreference electrode, unless otherwise noted. Oxygen was removed from the working solutions by purging with nitrogen gas. A ferrocene/ferrocenium redox couple was used as an internal standard, and the potential values obtained in reference to the silver electrode were converted to the vacuum scale.

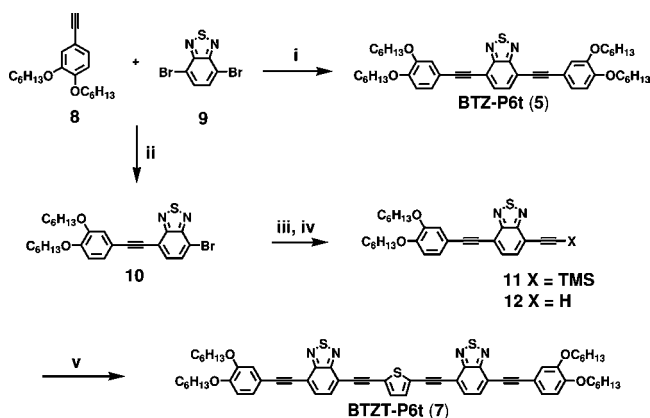
Thermal Characterization. Thermogravimetric analysis (TGA) was performed on a TA Q50 instrument at a ramp rate of 10 °C/min under N_2 (ramp: 25 to 800 °C) at atmospheric pressure in a platinum crucible.

Device Fabrication and Measurements. OFET Devices. Prime-grade n-doped silicon wafers having 300 nm thermally grown oxide (Process Specialties Inc.) were used as device substrates. Before film deposition, the substrates were cleaned by ultrasonic treatment with ethanol and then in an oxygen plasma cleaner for 5 min under vacuum. Films of compounds **1–7** were spin-coated from 0.5% (w/v) CHCl_3 , toluene, or chlorobenzene solutions and, if annealed, heated under nitrogen at various temperatures from 40° to 120 °C for 3 h. Spin-coated films were 25–30 nm thick as determined by profilometry (Tencor P10). For FET device fabrication, top contact gold electrodes (50 nm thickness) were deposited by thermal evaporation through a shadow mask. TFT device measurements were carried out at 21–23 °C in a customized high-vacuum probe station (1×10^{-6} Torr) or in air. Coaxial and/or triaxial shielding was incorporated into Signaton probes to minimize noise levels. TFT characterization was performed with a Keithley 6430 sub-femtoamperometer (drain) and Keithley 2400 (gate) source meter, operated by a locally written Labview program and GPIB communication. OFET response parameters were extracted from $I-V$ data using a standard field-effect transistor equation.³⁷ Mobilities (μ) were calculated in the saturation regime by the standard relationship: $\mu_{\text{sat}} = (2I_{\text{DS}}L)/[WC_i(V_G - V_T)^2]$, where I_{DS} is the source–drain saturation current, C_i is the gate dielectric capacitance (per area), V_G is the gate voltage, and V_T is the threshold voltage. The latter can be estimated as the intercept of the linear section of the plot of V_G vs $(I_{\text{DS}})^{1/2}$.

OPV Devices. These devices were fabricated by spin-coating a blend of **1–7** + PCBM (D:A wt:wt ratio, D = 1, 2; A = 1, 3), sandwiched between a transparent anode and a cathode. The anode consisted of glass substrates precoated with indium–tin oxide (ITO, Delta Technologies; $R_s = 8\text{--}12 \Omega/\square$). Before device fabrication, the ITO-coated (150 nm) glass substrates were cleaned by ultrasonic treatment with deionized water + detergent, deionized water, isopropyl alcohol, methanol, and acetone sequentially, and finally in a UV-ozone cleaner for 30 min under ambient atmosphere. A thin layer (30 nm) of PEDOT/PSS (Baytron P VP A1 4083) was spin-coated on (4000 rpm, 1 min) to modify the ITO surface. After baking at 150 °C for 15 min, the active layer was obtained by spin-coating the D:A blends under air at 6000 rpm (60 s) for **A-P6t**, **PA-P6t**, **A-P6d**, and **PA-P6t** (solution concentration: 16 mg/mL for **A-P6t**, **PA-P6t**, and **PA-P6t**, and 8 mg/mL for **A-P6d**); 2000 rpm (60 s) for **BTZ-P6t** and **BTZT-P6t** (8 mg/mL); and 4000 rpm (60 s) for **TBTZ-P6t** (8 mg/mL). Dry chloroform was used as the solvent. Contact areas were cleaned with dry toluene and a cotton swab; the thickness of the active layer film was measured by profilometry (Tencor, P10). The cathode consisted of LiF (~0.12 nm, Acros, 99.98%) capped with Al (150 nm, Sigma-Aldrich, 99.999%). The deposition rates used were 0.1 Å/s for LiF and ~2 Å/s for Al, with a chamber pressure of 1.1×10^{-6} Torr. Device characterization³⁸ was performed at 298 K using a Class A Spectra-Nova Technologies solar cell analyzer having a xenon lamp that simulates AM1.5G light from 400–1100 nm. The instrument was calibrated with a monocrystalline Si diode fitted with a KG3 filter to bring spectral mismatch to unity. The calibration standard was calibrated by the National Renewable Energy Laboratory (NREL). Four-point contacts were made to the substrate with Ag paste and copper alligator clips. Individual devices were isolated by a mask during testing to avoid current collection from adjacent devices and edge effects. Power conversion efficiencies were calculated from the following equation: $\text{PCE} = (J_{\text{sc}}V_{\text{oc}}\text{FF})/P_0$, where J_{sc} (mA/cm²)

(37) Sze, S. M. *Physics of Semiconductor Devices*, 2nd ed.; John Wiley & Sons: Taipei, Taiwan, 1981.

(38) (a) Silvestri, F.; Lopez-Duarte, I.; Seitz, W.; Beverina, L.; Martinez-Diaz, M. V.; Marks, T. J.; Guldi, D. M.; Pagani, G. A.; Torres, T. *Chem. Commun.* **2009**, 30, 4500–4502. (b) Irwin, M. D.; Buchholz, B.; Hains, A. W.; Chang, R. P. H.; Marks, T. J. *Proc. Natl. Acad. Sci. U.S.A.* **2008**, 105, 2783. (c) Hains, A. W.; Marks, T. J. *Appl. Phys. Lett.* **2008**, 92, 023504.

Scheme 1. Synthesis of Benzothiadiazole-Based Compounds **BTZ-P6t** and **BTZT-P6t**^a

^a (i) Pd(Ph₃P)₄/CuI, diisopropylamine, PhMe, 50 °C, 80%; (ii) Pd(Ph₃P)₄/CuI, diisopropylamine, PhMe, 50 °C, 51%; (iii) trimethylsilylacetylene, Pd(Ph₃P)₄/CuI, diisopropylamine, PhMe, 50 °C, 93%; (iv) Bu₄NF, THF, 25 °C, 89%; (v) 2,5-dibromothiophene, Pd(Ph₃P)₄/CuI, diisopropylamine, PhMe, 50 °C, 55%.

is the short circuit current, V_{oc} (V) the open circuit voltage, FF the fill factor, and P_0 the power of incident light source (mW/cm²).

Thin Film Characterization. Thin films were analyzed by wide-angle X-ray film diffractometry (WAXRD) on a Rigaku ATX-G instrument using standard θ - 2θ techniques with Cu K α_1 radiation. Atomic force microscopy was performed on a Jeol 5200 SPM instrument with silicon cantilevers in the tapping mode. Optical absorption spectra were acquired on a Shimadzu 1601 spectrophotometer.

Results

In the following sections, we report the synthesis as well as physical and electronic structure properties of semiconductors **1–7** as defined by thermal analysis, UV-vis optical spectroscopy, and cyclic voltammetry (CV). Next, the fabrication and characterization of **1–7**-based thin film transistors and bulk heterojunction solar cell devices are reported, and device response trends discussed in terms of molecular and electronic structure as well as film microstructure and morphology.

Semiconductor Synthesis. Compounds **A-P6t**, **PA-P6t**, **A-P6d**, and **TBTZ-P6t** were synthesized as described previously,^{14,15} while Scheme 1 details the synthetic routes to new compounds **BTZ-P6t** and **BTZT-P6t**. Pd(Ph₃P)₄/CuI-catalyzed Sonogashira coupling of 4,7-dibromo-2,1,3-benzothiadiazole **9**³⁹ with terminal alkyne **8**⁴⁰ affords compound **BTZ-P6t** in high yield (80%). The synthesis of compound **BTZT-P6t** begins with selective coupling between 4,7-dibromo-2,1,3-benzothiadiazole **9** and the alkyne **8** in toluene/diisopropylamine. The resulting bromo derivative **10** is then subjected to additional coupling with trimethylsilylacetylene, followed by deprotection of TMS-derivative **11** to provide intermediate **12**. Further coupling between 2,5-dibromothiophene and **12** affords target compound **BTZT-P6t** in good yield (55%).

Molecular Characterization. Thermal Properties. Thermogravimetric analysis (TGA, heating ramp rate = 10 °C/min under N₂) was used to assess the thermal stability of compounds **1–7** (Charts 4 and 5, Figure S1). The thermolysis onset

temperatures are found to be between 230 and 316 °C. Compared to many other molecular semiconductors used in organic electronics,⁴¹ this entire set of compounds is sufficiently thermally stable to be processed at typical OFET/OPV solution fabrication temperatures.

The anthracene-based semiconductors **A-P6t** and **PA-P6t** exhibit well-defined decomposition temperatures, comparable to those of the olefinic analogues **A-P6d** and **PA-P6d**. In contrast, 2,1,3-benzothiadiazole-based derivative **BTZ-P6t** exhibits a lower decomposition temperature ($T_d \approx 230$ °C) than semiconductors **TBTZ-P6t** and **BTZT-P6t**.

In addition to information about thermal decomposition processes, melting points provide insight into the cohesive energetics of intermolecular interactions in the solid state. As might be expected, compounds **PA-P6t** and **PA-P6d** exhibit higher melting temperatures than the related derivatives **A-P6t** and **A-P6d**, reflecting the increased molecular weight and extended π -conjugation (Chart 4). Within the pair **A-P6t** and **A-P6d**, the melting point decrease for fully *trans*¹⁴ olefinic compound **A-P6d** relative to the acetylenic analogue can be ascribed to a sterically related^{27a} twist of the conjugated backbone (*vide infra*), which results in less effective molecular packing, despite the greater polarizability of double over triple bonds. For the **PA-P6t** + **PA-P6d** couple, we tentatively ascribe the increased melting point of fully *trans*¹⁴ olefinic **PA-P6d** to the fact that in this case intermolecular cohesive forces due to the double bond polarizability⁴² are greater than those in parent structure **A-P6d**, due to the presence of two coplanar phenylene-vinylene moieties, which may overcome the aforementioned steric repulsions. Compounds **BTZ-P6t** and **TBTZ-P6t** exhibit similar melting points (Chart 5); such behavior may be ascribed to similar structural dimensions. Indeed, the relatively low melting point of compound **TBTZ-P6t** may indicate that it is conformationally more flexible than might be predicted from the number of possible repulsive intramolecular interactions.⁴² Compound **BTZT-P6t** has the highest melting point within the BTZ-based semiconductor series, reflecting the collective effects of increased molecular weight, extended effective conjugation, and enhanced donor-acceptor interactions (Chart 5).

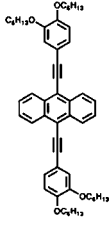
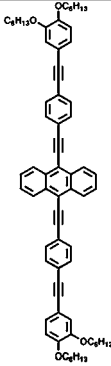
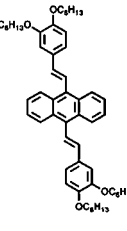
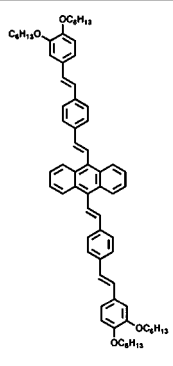
Optical Absorption Spectroscopy. Characterizing the optical absorption cross sections of compounds **1–7** is essential for photovoltaic studies and was performed both in chloroform solution and as thin films (Figure S2). Charts 4 and 5 summarize the data for all compounds. The thin film spectra of **1–7** are red-shifted relative to the solution spectra, which can be attributed to greater structural organization in the solid state. Note from Chart 4 that the λ_{soln} and λ_{film} longest wavelength absorption maxima for the anthracene-based semiconductors fall in the order **PA-P6t** > **A-P6t** > **A-P6d** > **PA-P6d** and **PA-P6t** > **A-P6t** > **PA-P6d** > **A-P6d**. Clearly, anthracene spacing with double vs triple bonds causes a significant twist of the conjugated backbone due to significant H(olefinic)-H(4-anthracene) nonbonded repulsions. This explains the ~ 40 nm blue shift of the absorption maximum of **A-P6d** and **PA-P6d** versus **A-P6t** and **PA-P6t**.^{27a,43} The coplanar structure and electron-withdrawing nature²⁷ of the $-C\equiv C-$ moieties are in accord with the smaller optical band gaps (E_g^{opt}) of compounds **A-P6t** and **PA-P6t**.

Regarding the benzothiadiazole-based semiconductors (Chart 5), both λ_{soln} and λ_{film} systematically fall in the order **TBTZ-P6t** > **BTZT-P6t** > **BTZ-P6t**. Introduction of a D-A-D motif in **TBTZ-P6t** and **BTZT-P6t** clearly results in red-shifted

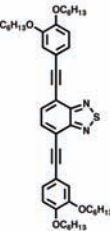
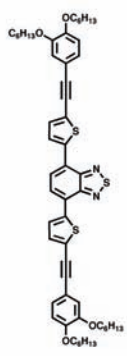
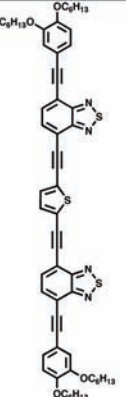
(39) Edelmann, M. J.; Raimundo, J.-M.; Utesch, N. F.; Diederich, F.; Boudon, C.; Gisselbrecht, J.-P.; Gross, M. *Helv. Chim. Acta* **2002**, *85*, 2195.

(40) Valentini, L.; Bagnis, D.; Marrocchi, A.; Seri, M.; Taticchi, A.; Kenny, J. M. *Chem. Mater.* **2008**, *20*, 32.

Chart 4. Melting Point (m.p.), Decomposition Temperature Onset (T_d), Solution (CHCl_3) and Thin-Film (Glass Substrate) Optical Absorption Maxima (λ), and Optical Energy Gap (E_g^{opt}) for Compounds **A-P6t**, **PA-P6t**, **A-P6d**, and **PA-P6d**^a

				
	A-P6t (1) ^a	PA-P6t (2) ^a	A-P6d (3) ^a	PA-P6d (4) ^a
m.p. (°C)	130-131	168-169	118-119	205-206
T_d (°C)	270	276	314	316
λ_{soln} (nm)	322, 457	350, 464, 486	317, 417	349, 423
log(ε_{max})	4.4, 4.6	4.7, 4.9, 4.8	4.4, 4.3	4.8, 4.7
(E_g^{opt})_{soln} (eV)	-2.25	-2.30	-2.39	-2.53
λ_{film} (nm)	439, 467, 503	366, 438, 481, 514	393, 448	357, 440

^a Data from ref 14.**Chart 5.** Melting Point (m.p.), Decomposition Temperature Onset (T_d), Solution (CHCl_3) and Thin-Film (Glass Substrate) Optical Absorption Maxima (λ), and Optical Energy Gap (E_g^{opt}) for Compounds **BTZ-P6t**, **TBTZ-P6t**, and **BTZT-P6t**^a

			
	BTZ-P6t (5)	TBTZ-P6t (6) ^a	BTZT-P6t (7)
m.p. (°C)	139-140	126-127	188-189
T_d (°C)	230	310	280
λ_{soln} (nm)	311, 447	359, 503	319, 328, 472
log(ε_{max})	4.6, 4.4	4.8, 4.6	4.8, 4.9, 5.0
(E_g^{opt})_{soln} (eV)	-2.43	-2.17	-2.24
λ_{film} (nm)	336, 445, 473	357, 481, 508, 563	335, 461, 486, 521

^a Data from ref 15.

absorption and reduces the optical band gap.⁴⁴ Note here also the red-shifted absorption maxima characteristic^{13b,45} of an-

thracene versus phenylene cores, leading to greater solar photon harvesting (*vide infra*). The origin of this shift is

Table 1. Electrochemical Data^a and MO Energies for Compounds 1–7

Compound	$E_{\text{ox}}^{1/2}$ (V) (ΔE)	$E_{\text{red}}^{\text{on}}$ (V)	E_{HOMO} (eV)	E_{LUMO} (eV)
A-P6t (1)^b	+0.64 (0.1)	—	-5.51	-2.98
PA-P6t (2)	—	-1.57	-5.44	-3.04
A-P6d (3)	+0.21 (0.2)	—	-5.01	-2.50
PA-P6d (4)	+0.41 (0.1)	—	-5.21	-2.70
BTZ-P6t (5)	—	-1.71	-5.52	-3.09
TBTZ-P6t (6)	+0.48 (0.06)	—	-5.33	-3.21
BTZT-P6t (7)	+0.69 (0.1)	—	-5.49	-3.35

^a Determined vs Fc/Fc⁺. ^b Electrochemistry performed on carbon working electrode.

π -topological^{45b}—anthracene has a lower optical gap than benzene—and reflects slightly increased π -delocalization along the principal molecular axis. Similarly, replacement of phenylene with a BTZ unit is expected to red-shift the absorption spectra.⁴⁶

Electrochemical Characterization. Cyclic voltammetry (CV) experiments with semiconductors 1–7 (Figure S3) were performed under N₂ in 0.1 M CH₂Cl₂/TBAPF₆ solutions. The redox potentials were measured versus the ferrocene/ferrocenium redox couple (Fc/Fc⁺), used as the internal reference. With the exception of compound **PA-P6t**, all systems exhibit reversible and/or quasi-reversible oxidation/reduction waves within the span of the solvent/electrolyte window. In cases where the voltammograms are (quasi)reversible, it is possible to extract half-wave potentials ($E^{1/2}$); data are summarized in Table 1.

Not surprisingly, acetylenic systems **A-P6t** and **PA-P6t** are more difficult to oxidize than corresponding olefinic **A-P6d** and **PA-P6d**, because the triple bond is less electron-rich.⁴⁷ Indeed, the oxidation potentials for **A-P6t** and **PA-P6t** are ~ 0.4 eV higher than those of the olefinic analogues (Figure S3). Moreover, the resistance of **A-P6t** and **PA-P6t** to oxidation not unexpectedly increases with decreasing conjugation length.⁴⁸ Correspondingly, it is somewhat more difficult to reduce **A-P6d** and **PA-P6d**, which is consistent with the greater electron richness. The HOMO and LUMO energies of semiconductors 1–7 were estimated from optical absorption and cyclic voltammetry data using the standard approximation that the Fc/Fc⁺ HOMO level is -4.8 eV.⁴⁹ These data are compiled in Table 1 and indicate that the HOMO energies of compounds 1–7 are within the required range to ensure very large V_{oc} values in

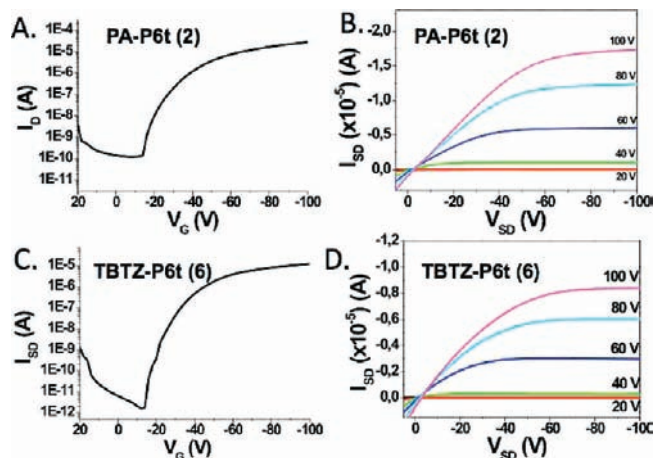


Figure 2. FET transfer (A) and output (B) plots for films of semiconductor **PA-P6t** spin-cast from chloroform onto Si/SiO₂ substrates and annealed at 120 °C, and semiconductor **TBTZ-P6t** (C and D, respectively) spin-cast from chloroform onto Si/SiO₂ substrates and annealed at 40 °C. Measurements made in vacuum.

PCBM BHJ photovoltaic cells. Note also that the LUMO energy levels for BTZ-based semiconductors 5–7 lie significantly below those of anthracene derivatives 1–4, reflecting the strong electron-accepting character of the BTZ fragment.

Optoelectronic Device Characterization. Field-Effect Transistors. The structure of the typical top-contact OFETs fabricated in this study is shown schematically in Figure 1A. These bottom-gate top-contact devices consist of an n⁺-Si gate-substrate, a 300 nm SiO₂ dielectric layer, an optimized surface treatment with a self-assembled monolayer, a spin-coated 1–7 semiconductor film (~ 30 – 40 nm), and vacuum-deposited 50 nm thick Au source and drain electrodes. Device fabrication and measurement details are given in the Experimental Section. Representative output and transfer characteristics of devices fabricated with compounds 1–7 are shown in Figure 2 and Figures S4–S11. Typical p-type organic semiconductor characteristics are observed for all compounds. Tables 2 and 3 summarize the FET performance response for the present semiconductors, including the charge carrier mobility (μ), on–off current ratio ($I_{\text{on}}/I_{\text{off}}$), turn-on voltage (V_{ON}), and threshold voltage (V_{T}).

To elucidate optimum semiconductor thin film growth conditions, chloroform solutions of 1–7 were spin-coated onto Si/SiO₂ substrates and then annealed at varying temperatures for 3 h before device completion. Thermal annealing from 40 to 80 °C generally enhances TFT performance. However, higher annealing temperatures (120 °C) are found to have detrimental effects (except for compounds **PA-P6t** and **PA-P6d**), although the T_{d} 's of 1–7 are greater than 230 °C (Chart 4). Device response maximizes at an annealing temperature of 80 °C for semiconductors **PA-P6t**, **BTZ-P6t**, **TBTZ-P6t**, and **BTZT-P6t** and at 60 °C for semiconductors **A-P6t**, **A-P6d**, and **PA-P6d**.

The data in Tables 2 and 3 reveal that compounds **PA-P6t** and **TBTZ-P6t** exhibit the highest FET mobilities, 0.07 and 0.02 cm² V⁻¹ s⁻¹, respectively,¹⁵ while all other semiconductors have significantly lower mobilities ($<10^{-3}$ cm² V⁻¹ s⁻¹). The $I_{\text{on}}/I_{\text{off}}$ ratios of **PA-P6t** and **TBTZ-P6t** are generally $\sim 10^5$ – 10^7 whereas those of the others semiconductors are lower ($\sim 10^2$ – 10^4). In general, semiconductor molecular architecture is the most critical factor in determining the nature and the degree of solid state order. However, for film fabrication from solution, the solvent properties greatly affect film nucleation

- (41) (a) Gao, J.; Li, L.; Meng, Q.; Li, R.; Jiang, H.; Li, H.; Hu, W. *J. Mater. Chem.* **2007**, *17*, 1421. (b) Xiao, K.; Liu, Y.; Qi, T.; Zhang, W.; Wang, F.; Gao, J.; Qiu, W.; Ma, Y.; Cui, G.; Chen, S.; Zhan, X.; Yu, G.; Qin, J.; Weping, H.; Zhu, D. *J. Am. Chem. Soc.* **2005**, *127*, 13281. (c) Li, X.-C.; Sirringhaus, H.; Garnier, F.; Holmes, A. B.; Moratti, S. C.; Feeder, N.; Clegg, W.; Teat, S. J.; Friend, R. H. *J. Am. Chem. Soc.* **1998**, *120*, 2206.
- (42) (a) Karthikeyan, M.; Glen, R. C.; Bender, A. *J. Chem. Inf. Model.* **2005**, *45*, 581. (b) Katritzky, A.; Lobanov, V.; Karelson, M. *Chem. Soc. Rev.* **1995**, *24*, 279.
- (43) Garay, R. O.; Naarmann, H.; Müllen, K. *Macromolecules* **1994**, *27*, 1922.
- (44) For other example of this phenomenon, see: Kron, R.; Lenes, M.; Hummelen, J. C.; Blom, P. W. M.; De Boer, B. *Polym. Rev.* **2008**, *48*, 531.
- (45) (a) Egbe, D. A. M.; Carbonnier, B.; Birckner, E.; Grummt, U.-W. *Prog. Polym. Sci.* **2009**, *34*, 1023–1067. (b) Schenning, A. P. H. J.; Tsipis, A. C.; Meskers, S. C. J.; Beljonne, D.; Meijer, E. W.; Bredas, J. L. *Chem. Mater.* **2002**, *14*, 1362.
- (46) Lu, S.; Yang, M.; Luo, J.; Cao, Y. *Synth. Met.* **2004**, *140*, 199.
- (47) (a) Thomas, T. D. *J. Chem. Phys.* **1970**, *52*, 1373. (b) Patai, S., Ed. *The Chemistry of the Carbon-Carbon Triple Bond*; J. Wiley and Sons: 1978.
- (48) LaRue, T. A.; Kurz, W. G. W. *Plant. Physiol.* **1973**, *51*, 1074.
- (49) Wu, C.-C.; Sturm, J. C.; Register, R. A.; Tian, J.; Dana, E. P.; Thompson, M. E. *IEEE Trans. Electron Devices* **1997**, *44* (8), 1269.

Table 2. FET Performance Parameters Measured under Vacuum and Air for Anthracene-Based Arylacetylenes **A-P6t**, **PA-P6t**, **A-P6d**, and **PA-P6d** Films Spin-Cast from the Indicated Solvents

Compound	Solvent	T_a (°C) ^a	μ (cm ² V ⁻¹ s ⁻¹)		I_{on}/I_{off}		V_{on} (V)		V_T (V)	
			Vac	Air	Vac	Air	Vac	Air	Vac	Air
A-P6t (1)	CHCl ₃	40	1×10^{-5}	-	3×10^3	-	-10	-	-9	-
	CHCl ₃	60	4×10^{-4}	3.9×10^{-4}	10^4	10^2	-3	-10	-8	-15
	CHCl ₃	80	no activity	-	-	-	-	-	-	-
PA-P6t (2)	Toluene	80	2×10^{-6}	-	10^2	-	-16	-	-23	-
	CB	80	8×10^{-7}	-	10^2	-	-12	-	-15	-
	CHCl ₃	40	2×10^{-2}	-	10^7	-	-30	-	-35	-
	CHCl ₃	60	3×10^{-2}	2×10^{-2}	10^5	7×10^4	-12	-14	-15	-20
	CHCl ₃	80	7×10^{-2}	7×10^{-2}	4×10^6	2×10^2	0	-22	-8	-22
A-P6d (3)	CHCl ₃	120	3×10^{-2}	-	10^5	-	-13	-	-17	-
	Toluene	80	2×10^{-6}	-	10^2	-	-19	-	-20	-
	CB	80	2×10^{-7}	-	<10	-	-27	-	-28	-
	CHCl ₃	40	2×10^{-7}	-	8×10^2	-	-9	-	-25	-
	CHCl ₃	60	3×10^{-4}	2×10^{-4}	10^4	2×10^3	-32	-14	-32	-16
PA-P6d (4)	CHCl ₃	80	2×10^{-5}	-	2×10^4	-	-10	-	-12	-
	Toluene	80	1×10^{-6}	-	10^2	-	-15	-	-17	-
	CB	80	2×10^{-6}	-	10^2	-	-9	-	-13	-
	CHCl ₃	40	2×10^{-6}	-	9×10^3	-	-14	-	-20	-
	CHCl ₃	60	3×10^{-4}	2×10^{-5}	10^4	6×10^5	-26	-23	-27	-25
BTZ-P6t (5)	CHCl ₃	80	4×10^{-5}	7×10^{-6}	10^3	10^2	-44	-46	-50	-52
	CHCl ₃	40	2×10^{-2}	-	10^7	-	-13	-	-20	-
	CHCl ₃	60	1×10^{-2}	-	10^5	-	-12	-	-13	-
	CHCl ₃	80	2×10^{-2}	2×10^{-2}	6×10^5	5×10^3	-3	-19	-7	-25
	Toluene	80	8×10^{-7}	-	10	-	-47	-	-53	-
TBTZ-P6t (6)	CB	80	3×10^{-6}	-	10^2	-	-14	-	-17	-
	CHCl ₃	40	no activity	-	-	-	-	-	-	-
	CHCl ₃	60	7×10^{-6}	-	8×10^1	-	-29	-	-30	-
	CHCl ₃	80	2×10^{-4}	2×10^{-5}	10^2	1×10^4	-24	-12	-30	-36
	CHCl ₃	120	no activity	-	-	-	-	-	-	-
BTZT-P6t (7)	Toluene	80	no activity	-	-	-	-	-	-	-
	CB	80	4×10^{-7}	-	10	-	-51	-	-55	-

^a T_a = annealing temperature.**Table 3.** FET Performance Measured Under Vacuum and Air for Benzothiadiazole-Based Arylacetylenes **BTZ-P6t**, **TBTZ-P6t**, and **BTZT-P6t** Films Spin-Cast from the Indicated Solvents

Compound	Solvent	T_a (°C) ^a	μ (cm ² V ⁻¹ s ⁻¹)		I_{on}/I_{off}		V_{on} (V)		V_T (V)	
			Vac	Air	Vac	Air	Vac	Air	Vac	Air
BTZ-P6t (5)	CHCl ₃	40	no activity	-	-	-	-	-	-	-
	CHCl ₃	60	3×10^{-6}	-	4×10^3	-	-10	-	-15	-
	CHCl ₃	80	4×10^{-5}	7×10^{-6}	10^3	10^2	-44	-46	-50	-52
TBTZ-P6t (6)	CHCl ₃	40	2×10^{-2}	-	10^7	-	-13	-	-20	-
	CHCl ₃	60	1×10^{-2}	-	10^5	-	-12	-	-13	-
	CHCl ₃	80	2×10^{-2}	2×10^{-2}	6×10^5	5×10^3	-3	-19	-7	-25
	Toluene	80	8×10^{-7}	-	10	-	-47	-	-53	-
	CB	80	3×10^{-6}	-	10^2	-	-14	-	-17	-
BTZT-P6t (7)	CHCl ₃	40	no activity	-	-	-	-	-	-	-
	CHCl ₃	60	7×10^{-6}	-	8×10^1	-	-29	-	-30	-
	CHCl ₃	80	2×10^{-4}	2×10^{-5}	10^2	1×10^4	-24	-12	-30	-36
	CHCl ₃	120	no activity	-	-	-	-	-	-	-
	Toluene	80	no activity	-	-	-	-	-	-	-
BTZT-P6t (7)	CB	80	4×10^{-7}	-	10	-	-51	-	-55	-

^a T_a = annealing temperature.

and growth mechanism and morphology, and thus charge transport properties.⁵⁰

Thus, Siringhaus et al.⁵¹ reported that P3HT TFT performance can be enhanced by using high-boiling solvents instead of chloroform for film growth. This is the result of the slower solvent evaporation, which facilitates the slow growth of highly crystalline films, thereby enhancing interchain interactions and charge mobility. For these reasons, solutions of **1–7** were also spin-coated using other solvents such as toluene (bp = 111 °C) and chlorobenzene (CB, bp = 131 °C). However, the smoothest,

most continuous, and most electrically uniform films were obtained here from chloroform solutions, generally resulting in the greatest FET performance (Tables 2 and 3). The poor quality of toluene and CB spun films appears to result from the lower solubility of these compounds in those solvents. In fact, in most cases, the compounds precipitate during solvent evaporation resulting in irregular films with areas of heavy deposition distinguishable by eye as islands of crystalline material.

OFET devices based on compounds **PA-P6t** and **TBTZ-P6t** were also fabricated by drop-casting 0.5% (w/v) chloroform solutions and then annealing at 80 °C under N₂ for 3 h. Using this methodology, the semiconductor films are irregular and discontinuous, displaying a negligible FET response (not shown). Finally, the devices affording the maximum perfor-

(50) Banach, M. J.; Friend, R. H.; Siringhaus, H. *Macromolecules* **2004**, *37*, 6079.

(51) Chang, J. F.; Sun, B.; Breiby, D. W.; Nielsen, M. M.; Solling, T. I.; Giles, M.; McCulloch, I.; Siringhaus, H. *Chem. Mater.* **2004**, *16*, 4772.

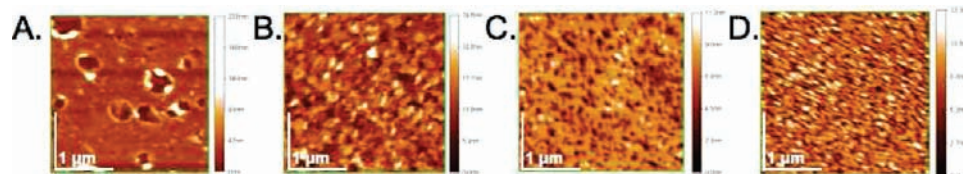


Figure 3. AFM images ($1\ \mu\text{m} \times 1\ \mu\text{m}$) of (A) **A-P6t** (60 °C), (B) **PA-P6t** (80 °C), (C) **A-P6d** (60 °C), and (D) **PA-P6d** (120 °C) films spin-cast from chloroform on Si/SiO₂ substrates and annealed at the indicated temperatures.

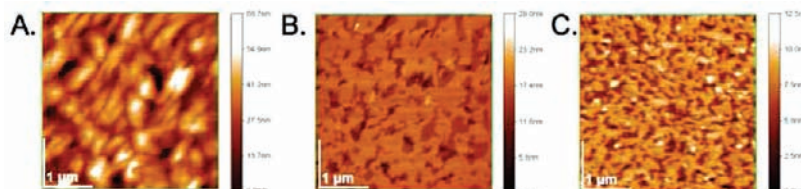


Figure 4. AFM images ($1\ \mu\text{m} \times 1\ \mu\text{m}$) of (A) **BTZ-P6t**, (B) **TBTZ-P6t**, and (C) **BTZT-P6t** films spin-cast from chloroform on Si/SiO₂ substrates and annealed at 80 °C.

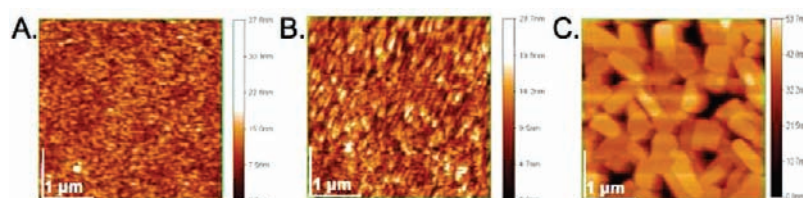


Figure 5. AFM images ($1\ \mu\text{m} \times 1\ \mu\text{m}$) of films of **PA-P6t** spin-cast from chloroform on Si/SiO₂ substrates and annealed at (A) 40 °C, (B) 60 °C, and (C) 120 °C.

mance were also evaluated in air, revealing no substantial changes in carrier mobilities (except for compound **BTZ-P6t**), whereas the $I_{\text{on}}/I_{\text{off}}$ ratio generally falls, likely due to O₂ doping as typically observed for electron-rich semiconductors such as oligothiophenes.⁵²

Atomic force microscopy (AFM) images were recorded to examine the morphologies of the **1–7** semiconducting films, and the results correlate well with the diffraction (*vide infra*) and TFT data. Figures 3 and 4 show AFM images of **1–4** and **5–7** films, respectively, deposited on bare SiO₂ and annealed at temperatures yielding the highest carrier mobilities. The **A-P6t**-derived films spin-cast from chloroform solution contain large circular holes in otherwise featureless surfaces (~ 20 nm rms roughness, σ ; Figure 3A). In contrast, arylacetylene **PA-P6t**-derived films exhibit large crystal-like features¹⁵ and an rms roughness of ~ 3.2 nm (Figure 3B). Finally, films of compounds **A-P6d**, **PA-P6d**, **TBTZ-P6t**,¹⁵ and **BTZT-P6t** are smooth ($\sigma = 1.27, 1.61, 2.05,$ and 1.19 nm, respectively) whereas films of **BTZ-P6t** are far rougher with a $\sigma = 8.55$ nm, which may be ascribed to the formation of segregated phases that inhibit efficient charge transport⁵³ and afford a significantly lower mobility.

As another example of film microstructure/morphology–mobility correlations, note how **PA-P6t**-based film roughness evolves with the annealing temperature (Figures 3B and 5). Increasing T_a from 40 to 60 to 80 °C induces a progressive increase in σ ($2.34 \rightarrow 2.68 \rightarrow 3.55$ nm, respectively) which correlates with increasing mobility ($0.02 \rightarrow 0.03 \rightarrow 0.07$ cm²

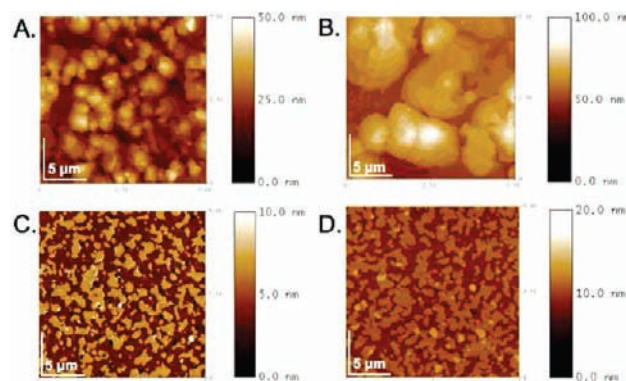


Figure 6. AFM images ($5\ \mu\text{m} \times 5\ \mu\text{m}$) of **PA-P6t**- and **TBTZ-P6t**-derived films spin-cast from toluene (A and C, respectively) and chlorobenzene (B and D, respectively).

V⁻¹ s⁻¹, respectively). These results argue that crystallization processes result in enhanced semiconductor film molecular self-organization. However, a different morphology is observed at higher annealing temperature (120 °C), with decreased film continuity, although the grain size increases, which explains the depressed mobility.

The morphologies of **1–7**-derived films spin-cast from chloroform are substantially different from those from toluene and CB. For example, Figure 6A shows the AFM image of **PA-P6t**-derived films spin-cast from toluene ($\sigma = 6.0$ nm), featuring grains with dimensions of ~ 200 nm and heights of tens of nanometers. The **PA-P6t**-derived films spin-cast from CB ($\sigma = 7.8$ nm) are similar, exhibiting taller as well as wider clusters (Figure 6B). Similarly, **TBTZ-P6t**-derived films spin-cast from toluene ($\sigma = 1.63$ nm) and CB ($\sigma = 1.75$ nm) exhibit large crystal-like features (Figure 6C and 6D, respectively). Note that films of **TBTZ-P6t** from CB solution exhibit more highly interconnected microstructures versus those from toluene. These

(52) (a) Meijer, E. J.; Detcher, C.; Baesjou, P. J.; van Veenendaal, E.; de Leuw, D. M.; Klapwijk, T. M. *J. Appl. Phys.* **2003**, *93*, 4831. (b) Bao, Z.; Dodabalapur, A.; Lovinger, A. *J. Appl. Phys. Lett.* **1996**, *69*, 4108.

(53) Kline, R. J.; McGehee, M. D.; Kadnikova, E. N.; Liu, J.; Frechet, J. M.; Toney, M. F. *Macromolecules* **2005**, *38*, 3312.

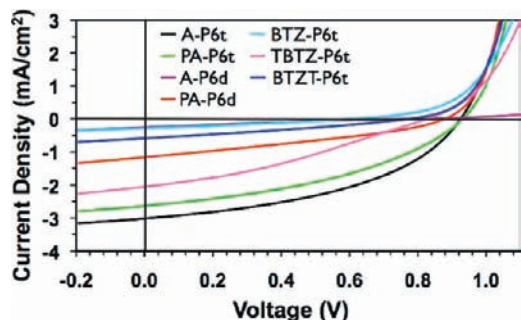


Figure 7. Current density (J)–Voltage (V) characteristics under illumination of optimized 1-7/PCBM based BHJ devices. **A-P6t/PCBM** 2:1 wt/wt (black), **PA-P6t/PCBM** 2:1 (green), **A-P6d/PCBM** 2:1 (violet), **PA-P6d/PCBM** 1:1 (red), **BTZ-P6t/PCBM** 1:1 (cyan), **TBTZ-P6t/PCBM** 1:1 (pink), **BTZT-P6t/PCBM** 1:1 (blue).

Table 4. Bulk Heterojunction Photovoltaic Response Properties of Compounds **A-P6t**, **PA-P6t**, **A-P6d**, and **PA-P6d**

Active layer [wt:wt]	V_{oc} [V]	J_{sc} [mA/cm ²]	FF [%]	PCE [%]	R_{sh} [KΩ/cm ²]
A-P6t/PCBM (1:1) ^{a,d}	0.96	2.62	45	1.17	29.4
A-P6t/PCBM (1:3) ^{a,d}	0.81	0.86	26	0.18	28.0
A-P6t/PCBM (1:3) ^{a,e}	0.74	0.76	26	0.15	16.1
A-P6t/PCBM (2:1) ^{a,d}	0.93	2.92	26	1.20	20.4
A-P6t/PCBM (2:1) ^{a,e}	0.89	3.10	45	1.27	20.8
PA-P6t/PCBM (1:1) ^{b,d}	0.93	2.63	41	1.02	11.9
PA-P6t/PCBM (1:3) ^{b,d}	0.66	0.65	38	0.17	33.1
PA-P6t/PCBM (1:3) ^{b,e}	0.65	0.82	40	0.21	28.9
PA-P6t/PCBM (2:1) ^{b,d}	0.95	2.57	48	1.20	38.9
PA-P6t/PCBM (2:1) ^{b,e}	0.89	2.02	48	0.88	27.6
A-P6d/PCBM (1:1) ^{a,d}	0.79	0.26	20	0.04	39.9
A-P6d/PCBM (1:3) ^{a,d}	0.76	0.45	24	0.08	30.9
A-P6d/PCBM (1:3) ^{a,e}	0.63	0.59	26	0.10	24.0
A-P6d/PCBM (2:1) ^{a,d}	0.72	0.49	24	0.08	27.1
A-P6d/PCBM (2:1) ^{a,e}	0.65	0.76	34	0.17	31.7
PA-P6d/PCBM (1:1) ^{c,d}	0.88	1.16	32	0.34	17.3
PA-P6d/PCBM (1:3) ^{c,d}	0.78	1.05	26	0.22	13.7
PA-P6d/PCBM (1:3) ^{c,e}	0.81	1.44	26	0.31	11.2
PA-P6d/PCBM (2:1) ^{c,d}	0.65	0.23	30	0.05	18.0
PA-P6d/PCBM (2:1) ^{c,e}	0.56	0.28	33	0.05	26.1

^a $d = 100$ nm. ^b $d = 50$ nm. ^c $d = 80$ nm. ^d Not annealed. ^e Annealed at 60 °C/1 h.

microstructural and morphology findings are in good agreement with the corresponding OFET data.

Bulk Heterojunction Solar Cells. The potential of semiconductors 1–7 as donor (D) materials in OPV devices was investigated in bulk-heterojunction (BHJ) cells using (6,6)-phenyl-C₆₁ butyric acid methyl ester (PCBM) as the electron acceptor (A). The device structure utilized, glass/ITO/PEDOT:PSS/DONOR:PCBM/LiF/Al, is illustrated in Figure 1B. The active layer films were spin-coated from dry chloroform solutions (chloroform was found to be the optimum solvent). Device fabrication details are given in the Experimental Section. OPV current density–voltage (J – V) plots under illumination for the optimized devices based on arylacetylenes 1–7 are shown in Figure 7.

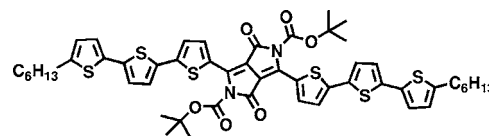
Tables 4 and 5 summarize the photovoltaic response data. The performance of these OPVs is clearly dependent on the donor material, blend composition, and film annealing temperature. For cells based on **A-P6t** and **PA-P6t/PCBM** in a 1:1 w:w ratio, power conversion efficiencies are 1.17 and 1.02%, respectively.¹⁴ When the D:A blend ratio is increased to 2:1, efficiencies rise to as high as 1.20%. However, further increasing the PCBM content in the **A-P6t** and **PA-P6t** blends (1:3 wt/wt) leads to a significant fall in the short circuit current densities (to 0.86 and 0.65 mA/cm², respectively) as well as in V_{oc} (to

Table 5. Bulk Heterojunction Photovoltaic Response Properties of Compounds **BTZ-P6t**, **TBTZ-P6t**, and **BTZT-P6t**

Active layer [wt:wt]	V_{oc} [V]	J_{sc} [mA/cm ²]	FF [%]	PCE [%]	R_{sh} [KΩ/cm ²]
BTZ-P6t/PCBM (1:1) ^{a,d}	0.66	0.28	27	0.05	71.1
BTZ-P6t/PCBM (1:3) ^{a,d}	0.53	0.16	38	0.03	101.2
BTZ-P6t/PCBM (2:1) ^{a,d}	0.45	0.12	51	0.03	146.7
TBTZ-P6t/PCBM (1:1) ^{b,d}	0.89	2.90	21	0.56	13.5
TBTZ-P6t/PCBM (1:3) ^{b,d}	0.83	0.97	25	0.21	14.9
TBTZ-P6t/PCBM (2:1) ^{b,d}	0.64	1.76	25	0.28	8.3
BTZT-P6t/PCBM (1:1) ^{c,d}	0.67	0.47	33	0.13	30.7
BTZT-P6t/PCBM (2:1) ^{c,d}	0.80	0.45	30	0.11	41.5
BTZT-P6t/PCBM (1:3) ^{c,d}	0.66	0.37	33	0.08	42.8

^a $d = 50$. ^b $d = 80$. ^c $d = 50$ nm. ^d Not annealed.

Chart 6. Structure of α,α -DH6TDPP



0.81 and 0.66 V, respectively), thus resulting in lower power conversion efficiencies (0.18% and 0.17%, respectively; Table 4 and Figure 4A). A similar trend in film composition vs performance is not uncommon. For example, Durrant et al.⁵⁴ studied the effect of blend composition for BHJ devices with films of regioregular P3HT + PCBM and found that the highest external quantum and power conversion efficiencies are achieved for a 1:1 D:A w:w composition. Further addition of PCBM (1:2 and 1:4 wt/wt) significantly reduces the efficiency. This was tentatively attributed to disruption of P3HT chain packing so that mobility and light absorption at longer wavelengths were decreased. More recently, Nguyen et al.⁵⁵ reported high-efficiency solar cells based on a α,α -DH6TDPP/PCBM BHJ structure in which the optimal donor:acceptor wt/wt ratio is 70:30. Also in this case, increasing amounts of PCBM (50:50 and 30:70 wt/wt) depress the device performance (Chart 6).

From the optical absorption spectra, AFM analysis, and mobility measurements of the various blends, Nguyen et al. concluded that a high donor concentration enhances light absorption by the chromophore and order in the microstructure, in addition to balancing hole–electron charge transport properties.

The present devices based on olefinic structures **A-P6d** and **PA-P6d** exhibit low power conversion efficiencies (0.04% and 0.34%, respectively) using a 1:1 wt/wt ratio with PCBM,¹⁴ and the efficiency could not be significantly improved by varying the acceptor loading (Table 4, Figure 8A). These additional, further optimized measurements supplement our previous preliminary report on acetylene-based BHJ blends,¹⁴ which are significantly more PV-efficient than those based on the olefinic donors.

The effect of donor–acceptor blend thermal annealing at various temperatures (50–120 °C) and for different times before device completion was also investigated. It is known that thermal annealing of polymer-based bulk heterojunction solar cells can significantly affect the blend morphology and microstructure and generally leads to an increased J_{sc} and fill factor, hence an

(54) Kim, Y.; Choulis, S. A.; Nelson, J.; Bradley, D. D. C.; Cook, S.; Durrant, J. R. *J. Mater. Sci.* **2005**, *40*, 1371.

(55) Tamayo, A. B.; Walker, B.; Nguyen, T.-Q. *J. Phys. Chem. C* **2008**, *112*, 11545.

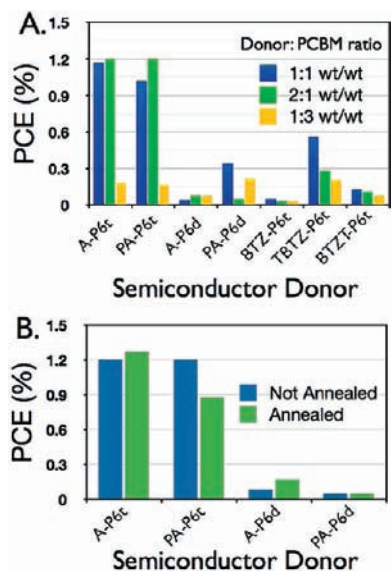


Figure 8. (A) OPV power conversion efficiencies for compound 1–7: PCBM BHJ cells as function of Donor:PCBM weight ratio. (B) Efficiencies for compound 1–4:PCBM (2:1 wt/wt) BHJ devices as function of thermal annealing at 60 °C/1 h.

increased PCE.⁵⁶ Indeed, for some of the materials investigated here, similar behavior is observed (Table 4). Thus, devices based on arylacetylenes **BTZ-P6t**, **TBTZ-P6t**, and **BTZT-P6t**, i.e., the systems containing benzothiadiazole units, exhibit lower PCEs vs those based on semiconductors **A-P6t** and **PA-P6t**.

The 1:1 weight ratio with respect to PCBM is found to be optimum; **TBTZ-P6t**-based devices exhibit better overall performance, especially in terms of the PCE approaching ~0.6% (Table 5, Figure 8A). After annealing at 60 °C, the short circuit current density for devices based on arylacetylene **A-P6t** (2:1 wt:wt with respect to PCBM) increases slightly from 2.92 to 3.1 mA/cm² and the fill factor (FF) from 26% to 45%. V_{oc} decreases slightly on annealing. As a result, the PCE increases from 1.20% to 1.27% (Table 4, Figure 8B). The PCEs of the devices based on the present acetylenic structures demonstrate how simple molecules can be efficient and competitive donor materials for small-molecule BHJ solar cells.^{55,57}

Thermal annealing of devices based on anthracenes **PA-P6t** and **PA-P6d** does not significantly affect the overall performance, whereas the **A-P6d**-based OPV performance is improved marginally upon annealing, to yield PCE ≈ 0.2%. In contrast, annealing of devices based on benzothiadiazoles **BTZ-P6t**, **TBTZ-P6t**, and **BTZT-P6t** leads to dramatic decreases in overall PV performance. When a higher PCBM ratio (1:1 or 1:3 wt/wt) is used, thermal annealing generally results in extensive film degradation, adversely affecting device performance.

The present OPVs generally exhibit good diode characteristics. For example, the **A-P6t**/PCBM blend cell, the current–voltage characteristics under illumination of which are shown in Figure 7, exhibit high rectification ratios under dark conditions (10^2 – 10^3 at 2.0 V, Figure 9). The other cells display similarly good rectification ratios (Figure 9).

It is known that film microstructure and morphology greatly influence OPV efficiency.^{12b,56} Figures 10A and S12 show AFM

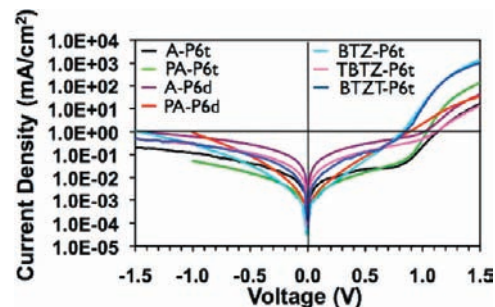


Figure 9. Dark J - V measurements for the 1–7/PCBM BHJ best devices. **A-P6t**/PCBM 2:1 wt/wt (black), **PA-P6t**/PCBM 2:1 (green), **A-P6d**/PCBM 2:1 (violet), **PA-P6d**/PCBM 1:1 (red), **BTZ-P6t**/PCBM 1:1 (cyan), **TBTZ-P6t**/PCBM 1:1 (pink), **BTZT-P6t**/PCBM 1:1 (blue).

images of Donor/PCBM blends having wt/wt ratios affording the best OPV performance. Films of **A-P6t**/PCBM and **PA-P6t**/PCBM in a 2:1 wt/wt ratio exhibit higher degrees of order than do **A-P6d** and **PA-P6d**/PCBM films having the same blend composition. These results are in accord with the significant torsional differences in the conjugated backbone when anthracene cores are connected with double versus triple bonds (*vide supra*), and this may inhibit self-organization. It is reasonable to argue that cooperative interactions between **A-P6t** (or **PA-P6t**) and PCBM occur, leading to a greater ordering, rather than aggregation of the donor molecules; this is in agreement with the similar solution and thin-film optical spectra observed for the two pristine compounds as well as the high V_{oc} values observed in **A-P6t**-**PA-P6t**/PCBM-based OPVs.⁵⁸ In contrast to the solution optical absorption spectra of pristine **A-P6d** and **PA-P6d**, their films are red-shifted, qualitatively indicating greater aggregation tendencies.⁵⁸ This may account for the lower V_{oc} values exhibited by the corresponding OPVs. Figure 10 shows AFM images of **A-P6t**/PCBM films as a function of the D/A ratio. Comparing the morphologies it is evident that films of **A-P6t**/PCBM 2:1 wt/wt ratio (Figure 10A) exhibit significantly higher order than do films of **A-P6t**/PCBM at 1:1 and 1:3 wt/wt ratios (Figure 10B and 10C, respectively). A similar trend is observed for **PA-P6t**–**PA-P6d**/PCBM blend films (Figures S12 and S13), with the 2:1 wt/wt ratio film revealing a higher degree of ordering.

Thermal annealing does not significantly affect the film morphology of either **A-P6t**/PCBM and **PA-P6t**/PCBM or **A-P6d**/PCBM and **PA-P6d**/PCBM as 2:1 wt/wt ratio blends (AFM images not shown). The slight effects observed on PCEs for 2:1 wt/wt **A-P6t**/PCBM and **A-P6d**/PCBM OPVs may be related to the energetic accessibility of molecular reorganization processes due to the shorter molecular length.

(56) (a) Liu, J.; Shi, Y.; Yang, Y. *Adv. Funct. Mater.* **2001**, *11*, 420. (b) Padinger, F.; Rittberger, R. S.; Sariciftci, N. S. *Adv. Funct. Mater.* **2003**, *13*, 85.

(57) (a) Liang, Y.; Feng, D.; Guo, J.; Szarko, J. M.; Ray, C.; Chen, L. X.; Yu, L. *Macromolecules* **2009**, *42*, 1091. (b) Ma, C.-Q.; Fonrodona, M.; Schicora, M. C.; Wienk, M. M.; Janssen, R. A. J.; Bäuerle, P. *Adv. Funct. Mater.* **2008**, *18*, 3323. (c) Lincker, F.; Delbosch, N.; Bailly, S.; De Bettignies, R.; Billon, M.; Pron, A.; Demadrille, R. *Adv. Funct. Mater.* **2008**, *18*, 3444. (d) Kronenberg, N. M.; Deppisch, M.; Würtnner, F.; Lademann, H. W. A.; Deing, K.; Meerholz, K. *Chem. Commun.* **2008**, 6489. (e) Silvestri, F.; Irwin, M. D.; Beverina, L.; Facchetti, A.; Pagani, G. A.; Marks, T. J. *J. Am. Chem. Soc.* **2008**, *130*, 17640. (f) He, C.; He, Q.; Yi, Y.; Wu, G.; Bai, F.; Shuai, Z.; Li, Y. *J. Mater. Chem.* **2008**, *18*, 4085. (g) Lloyd, M. T.; Mayer, A. C.; Subramanian, S.; Mourey, D. A.; Herman, D. J.; Bapat, A. V.; Anthony, J. E.; Maillaras, G. G. *J. Am. Chem. Soc.* **2007**, *129*, 9144. (h) Kopidakis, N.; Mitchell, W. J.; Lagemaat, J. V. d.; Ginley, D. S.; Rumbles, G.; Shaheen, S. E. *Appl. Phys. Lett.* **2006**, *89*, 103524. (i) Walker, B.; Tamayo, A. B.; Dang, X.-D.; Zalar, P.; Seo, H. J.; Garcia, A.; Tantiwiwat, M.; Nguyen, T.-Q. *Adv. Funct. Mater.* **2009**, *19*, 1–7. (58) Perez, M. D.; Borek, C.; Forrest, C.; Thompson, M. E. *J. Am. Chem. Soc.* **2009**, *131*, 9281.

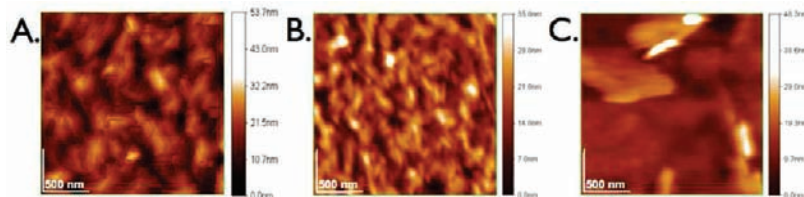


Figure 10. AFM images (500 nm \times 500 nm) of A-P6t/PCBM in (A) 2:1, (B) 1:1, (C) 1:3 wt/wt ratios.

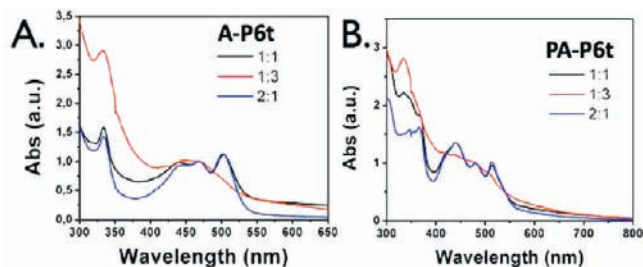


Figure 11. Thin film optical spectra of (A) A-P6t/PCBM and (B) PA-P6t/PCBM in 2:1 (blue line), 1:1 (black line), and 1:3 (red line) wt/wt ratios.

As judged by AFM, the 2:1 wt/wt A-P6t/PCBM and PA-P6t/PCBM blend films in general exhibit higher degrees of organization than 5-7/PCBM BHJ films. Anthracene-based arylacetylenes A-P6t and PA-P6t possess higher structural symmetry than do BTZ-based arylacetylenes 5–7, which may enhance supramolecular organization in BHJ blends. Within the BTZ-derivative series (Figures S12 and S14), the presence of the coplanar D–A–D motif in **TBTZ-P6t** may promote better self-organization, which is consistent with the greater current densities observed in the **TBTZ-P6t**-containing blends (Table 5). Additionally, the high V_{oc} values may also reflect the lower aggregation tendency of the pristine donor material, also evident in the similarity of the solution and thin film optical spectra⁵⁸ (*vide infra*).

The optical absorption spectra of the 1–7/PCBM blend films were also examined in detail. By increasing the blend D:A weight ratios, enhancement in the long wavelength optical absorption is observed (for representative spectra see Figures 11 and S15). This is beneficial for sunlight harvesting, since the photon flux reaching the earth's surface is maximum at ~ 1.8 eV (700 nm).⁵⁹ The enhanced long wavelength absorption by the A-P6t/PCBM and PA-P6t/PCBM blends (Figure 11) correlates with higher device efficiencies. At higher PCBM content (1:3), the absorption at wavelengths longer than 400 nm is strongly suppressed, while absorption in the blue region is maintained, suggesting that donor molecule dilution by the additional PCBM disrupts donor molecular packing and reduces the density of aggregates giving rise to red absorption.⁵⁴ These results correlate with the poor light harvesting at longer wavelengths observed for the high-PCBM content blends (*vide infra*).

Discussion

In this section we discuss OFET and OPV response characteristics within the context of the foregoing molecular structure discussion as well as the active semiconductor/blend film microstructure as assayed by wide-angle X-ray diffraction (WAXRD). For the OFETs, particular attention will focus on the semiconductor molecular orientation in the film and on

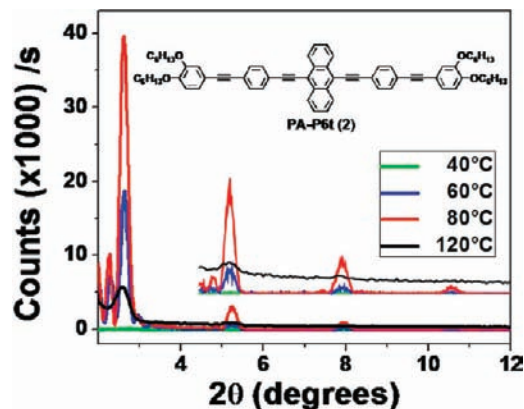


Figure 12. XRD plots for films of semiconductor PA-P6t (2) annealed at 40 °C (green line), 60 °C (blue line), 80 °C (red line), and 120 °C (black line).

Table 6. Summary of Diffraction-Derived d -Spacings (d), Computed Molecular Lengths (l), and Calculated Molecular Long Axis Tilt Angles (φ) in Semiconducting Films of Compounds 1–7 Spin-Cast from Chloroform Solution

Semiconductor	d -spacing (d , Å) ^a	molecular length ^b (l , Å)	tilt angle ^c (φ , deg)
A-P6t (1)	15.24	33.25	62.72
PA-P6t (2) ^d	34.20	46.33	42.42
A-P6d (3)	26.34	32.03	34.68
PA-P6d (4)	33.42	42.76	38.60
BTZ-P6t (5)	26.74	32.50	34.64
TBTZ-P6t (6) ^d	31.10	38.27	35.65
BTZT-P6t (7)	30.43	47.05	49.70

^a Minority phases are not reported. ^b Semiempirical AM1 calculations. ^c With respect to the substrate normal. $\varphi = \cos^{-1}(d/l)$. ^d Data from ref 15.

polycrystalline film grain connectivity. For the OPVs, the effect of donor molecular orbital energetics on key OPV parameters is studied in detail.

FET Performance vs Semiconductor Film Microstructure and Morphology. The highest mobility (hole mobility = 3×10^{-2} cm² V⁻¹ s⁻¹ and I_{on}/I_{off} ratio of $\sim 10^6$, Table 3) is found for films of semiconductor PA-P6t deposited from chloroform solution on Si/SO₂ and annealed at 80 °C. This behavior correlates well with high film crystallinity, indicated¹⁵ by the relatively high peak intensities in the out-of-plane X-ray diffraction data (Figure 12). The molecular long axis is tipped with respect to the substrate normal with a tilt angle $\theta \approx 40^\circ$ (Table 6), providing a plausible pathway for charge transport. Compound PA-P6t has almost the same core and side-chain molecular structure as A-P6t except that two phenylene-ethynylene units extend the backbone conjugation, which may favor more extensive π - π stacking in the solid state.⁶⁰

(60) (a) Hutchinson, G. R.; Ratner, M. A.; Marks, T. J. *J. Am. Chem. Soc.* **2005**, *127*, 16866. (b) Hutchinson, G. R.; Ratner, M. A.; Marks, T. J. *J. Phys. Chem. B* **2005**, *109*, 3126.

(59) Moliton, A.; Nunzi, J.-M. *Polym. Int.* **2006**, *55*, 583.

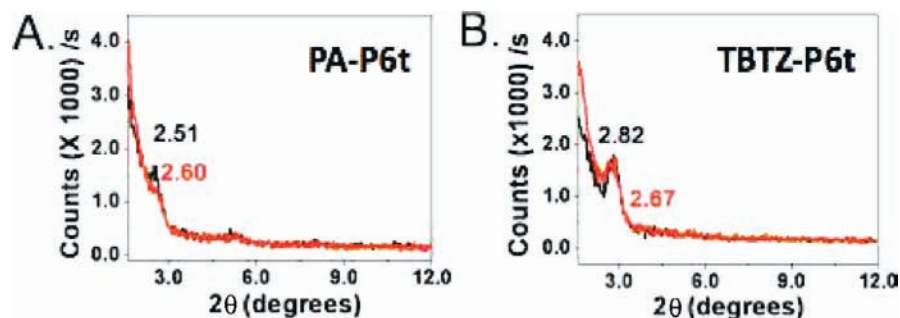


Figure 13. θ - 2θ X-ray diffraction data for films of (A) semiconductor **PA-P6t** (2) and (B) semiconductor **TBTZ-P6t** (6) spin-coated from toluene (black line) and chlorobenzene (red line) and annealed at 80 °C.

Interestingly, the FET response data reveal very different electrical behaviors compared to the **A-P6t**-based FETs. The highest measured **A-P6t** film mobility is 100 \times lower than that of **PA-P6t**. The **A-P6t** film XRD scans (Figure S16) exhibit a single low-intensity reflection corresponding to a d -spacing of 15.24 Å. The estimated molecular or long axis tilt angle φ with respect to the surface normal, defined by the d -spacing and computed molecular length (Table 6), is $\sim 63^\circ$, indicating that the molecules of **A-P6t** are tipped significantly from the surface normal. This is consistent with the observed poor FET mobilities. Upon replacing acetylenic for olefinic spacers in the **PA-P6t** molecular skeleton, a marked decrease in the carrier mobilities as well as I_{on}/I_{off} ratio is observed for optimized **PA-P6d** film-based TFTs (CHCl_3 , $T_a = 120^\circ\text{C}$) relative to those of **PA-P6t**, while the performance of **A-P6d** is only slightly lower than that of **A-P6t** (Table 2).

It is known⁶¹ that constraining conformational mobility arising from bond rotation is a viable molecular design concept for enhancing organic semiconductor mobility. The rotational degrees of freedom in acetylenes **A-P6t** and **PA-P6t** are minimal,⁶² compared to the corresponding olefins **A-P6d** and **PA-P6d**, and this should favor closer molecular packing and partially accounts for the superior FET performance. Additionally, the twisted conjugated backbones in **A-P6d** and **PA-P6d** (*vide supra*) may sterically hinder π - π stacking in the solid state. The diffraction data indicate that **PA-P6d** films have poor crystallinity, with only a broad second-order Bragg peak (Figure S16). Film quality is also poor for semiconductor **A-P6d** (Figure S16), which exhibits multiple film diffraction features, and a major reflection at $2\theta = 3.35^\circ$ (d -spacing = 26.34 Å, Table 6). The estimated tilt angles of these molecular structures are similar to that of **PA-P6t**, suggesting predominant edge-on molecular orientation on the substrate surface with a modest inclination.

The hole mobilities and the I_{on}/I_{off} ratios for arylacetylenes **A-P6t** and **PA-P6t** are generally greater than those of the benzothiadiazole-based materials, yielding the best performing OFETs, excepting compound **TBTZ-P6t** (Figure S17) for which the optimized performance (CHCl_3 , $T_a = 80^\circ\text{C}$) is similar to that of **PA-P6t**. This difference may be attributed to the higher structural symmetry of **A-P6t** and **PA-P6t**, which should *a priori* induce closer packing. The core geometry in **TBTZ-P6t** is to some degree fixed due to short intermolecular $\text{S}\cdots\text{N}$ contacts which should minimize any disorder caused by the benzothiadiazole ring rotation and favor close intermolecular π - π interactions. The regular structural organization in **TBTZ-P6t** is evident¹⁵ in the X-ray diffraction data (Figure 12) and

correlates with the similar mobilities observed for **PA-P6t**- and **TBTZ-P6t**-derived films.

The out-of-plane film microstructure is poor for benzothiadiazole-based materials **BTZ-P6t** and **BTZT-P6t** (Figure S16). **BTZ-P6t** films exhibit a single major reflection at $2\theta = 3.30^\circ$, corresponding to a d -spacing of 26.74 Å. Arylacetylene **BTZT-P6t** exhibits multiple diffraction features after annealing at 80 °C, with a major feature at $2\theta = 2.90^\circ$ corresponding to a d -spacing of 30.43 Å. With the calculated molecular lengths and XRD data taken into account (Table 6, Figure S16), arylacetylene **BTZT-P6t** exhibits a poorly ordered, edge-on orientation relative to the substrate surface with a tilt angle $\varphi \approx 50^\circ$.

Thermal annealing clearly affects performance (Tables 2 and 3), as exemplified by the results for the **PA-P6t**-derived films in Figure 12. On increasing the annealing temperature from 40 to 80 °C, the crystallinity and field-effect mobility of the films increase (μ by $\sim 3.5\%$; Table 2). Further increase of the annealing temperature to 120 °C lowers the crystallinity and, consequently, the mobility to the 40 °C value. Thus, annealing at $\sim 80^\circ\text{C}$ is optimum for this particular arylacetylene. The FET performance of the **1-7**-derived films generally exhibits marked casting solvent dependence (Tables 2 and 3). For example, TFTs fabricated from **PA-P6t**-derived films spin-coated from toluene solution show hole mobilities 4 orders of magnitude lower than those from films spin-coated from chloroform solution. Compound **PA-P6t** exhibits the lowest measured mobility of $2 \times 10^{-7} \text{ cm}^2 \text{ V}^{-1} \text{ s}^{-1}$ with $I_{on}/I_{off} < 10$ for films spin-coated from CB solution. Similarly, a very poor performance is obtained from devices fabricated with semiconductor **TBTZ-P6t** spin-coated from chlorobenzene and toluene, with hole mobilities 10^4 - $10^5\times$ lower, respectively, than those for devices spin-coated from a chloroform solution. The very low mobilities of thin films of **PA-P6t** and **TBTZ-P6t** spin-coated from toluene or CB correlate well with the XRD data (Figure 13), which exhibit extremely weak diffraction features, thus revealing little or no long-range order. These results argue that the degree of crystallinity is, not unexpectedly, a major factor in determining the measured carrier mobility in these compounds.

OPV Device Performance, Donor MO Energetics, and 1-7/PCBM Blend Morphology. Regarding OPV responses, the most efficient semiconductor donors discovered here are anthracene-based arylacetylenes **A-P6t** and **PA-P6t**, with PCEs up to $\sim 1.3\%$. These high efficiencies reflect good J_{sc} ($\sim 3.0 \text{ mA/cm}^2$) and exceptionally high V_{oc} values ($\sim 0.9 \text{ V}$). In contrast, the PCEs for **A-P6d/PCBM** and **PA-P6d/PCBM** (2:1 and 1:1 wt/wt, respectively)-based devices are poor, with lower J_{sc} and V_{oc} values. As previously communicated,¹⁴ the lower J_{sc} values for the olefinic semiconductors **A-P6d** and **PA-P6d** relative to

(61) Shirota, Y.; Kageyama, H. *Chem. Rev.* **2007**, *107*, 953.

(62) Zheng, S.-L.; Lin, N. A.; Reid, S.; Wang, B. *Tetrahedron* **2007**, *63*, 5427.

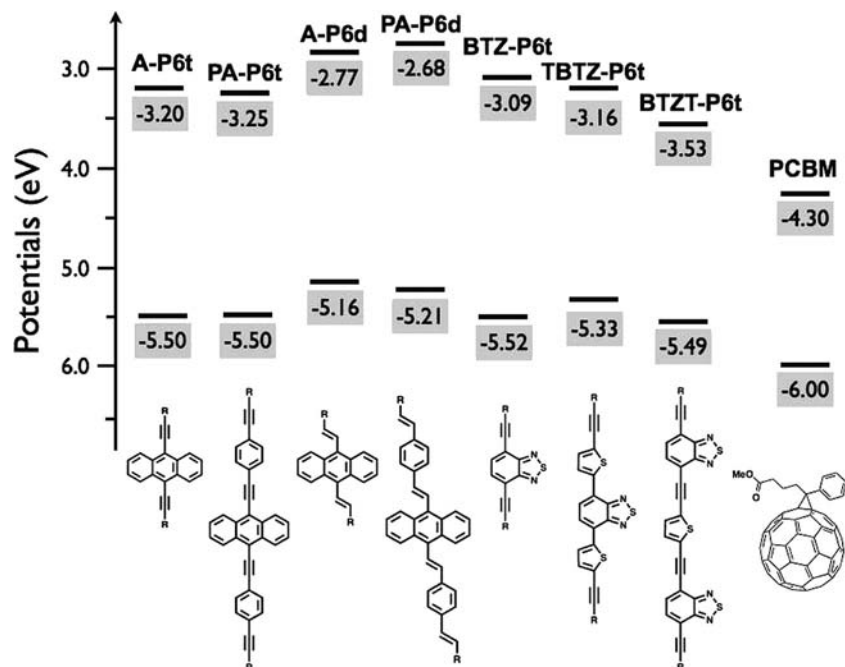


Figure 14. HOMO/LUMO energetics of donor derivatives 1–7 and the PCBM acceptor estimated from CV and optical data.

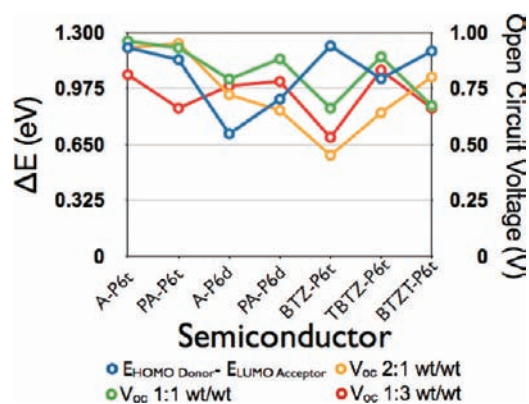


Figure 15. Energy difference (ΔE) between the HOMO level of donors 1–7 and LUMO level of PCBM *vs* V_{oc} values of BHJ OPVs made with blends having the indicated D:A weight ratios.

acetylenic **A-P6t** and **PA-P6t** correlate with the OFET hole mobilities, while the lower V_{oc} values may be attributed at least in part to the HOMO energies, which are ~ 0.2 eV higher for the olefinic donors (Figure 14). Within the BTZ-series, the **TBTZ-P6t**-based devices afford the greatest OPV performance, with the PCE approaching 0.6%. No significant correlations emerge from the HOMO/LUMO energetics–PCE metrics within this donor series (Figure 14) whereas V_{oc} clearly scales with the HOMO energy. We find here that V_{oc} for donors 1–7/PCBM BHJ OPVs is correlated with the energy difference (ΔE) between the donor HOMO and the PCBM LUMO, as shown in Figure 15, rather with the oxidation potentials.⁶³ Indeed, by changing the D/A weight ratio, it is necessary to consider the influence of other parameters such as morphology, photon absorption/loss, and exciton diffusion length.

As already noted, good active layer transport properties are important for efficient photovoltaic responses. To avoid important photocurrent loss by recombination, a hole mobility $\geq 10^{-3}$

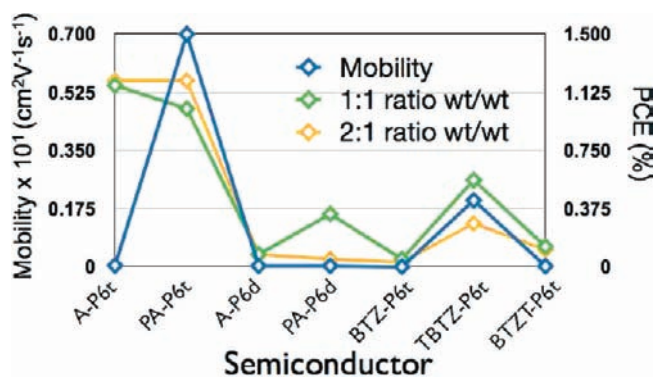


Figure 16. Correlation between semiconductor FET mobility (left y-axis, blue line) and BHJ OPV Photon to Current Efficiency (PCE, right y-axis) for the 1–7/PCBM based series of materials (green and orange lines indicate PCE values for D:A ratio = 1:1 and 2:1 wt/wt, respectively).

$\text{cm}^2 \text{V}^{-1} \text{s}^{-1}$ is generally considered necessary for the donor conjugated molecule/polymer.⁶⁴ The hole mobilities of semiconductors 1–7 correlate well with their OPV performance, except for compound **A-P6t**. We tentatively ascribe the different behavior of **A-P6t**/PCBM-based devices to the predominant effects of the active layer morphology (see above), as well as the donor MO energetics. Figure 16 shows how enhanced mobility correlates well with a higher photovoltaic response.

Spectral response data for the most efficient of the present OPVs are shown in Figures 17 and S18. Plots for devices fabricated using nonoptimal PCBM content are included for comparison. For **A-P6t**/PCBM 2:1 wt/wt films (Figure 17A) the EQE maximum is lower ($\sim 13\%$ at 550 nm) than that obtained for devices based on a 1:1 wt/wt blend ($\sim 27\%$ at 430 nm);¹⁴ however the 2:1 spectral response exhibits a broader profile. This may account^{12b} for the appreciably high J_{sc} response of the 2:1 vs 1:1 device (3.1 vs 2.6 mA/cm^2 , respectively).

Additionally, significantly lower EQE values in the 400–500 nm wavelength range are exhibited for devices based on **A-P6t**:

(63) Gadisa, A.; Svensson, M.; Andersson, M. R.; Inganäs, O. *Appl. Phys. Lett.* **2004**, *84*, 1609–1611.

(64) Wakim, S.; Aich, B.-R.; Tao, Y.; Leclerc, M. *Polym. Rev.* **2008**, *48*, 1558.

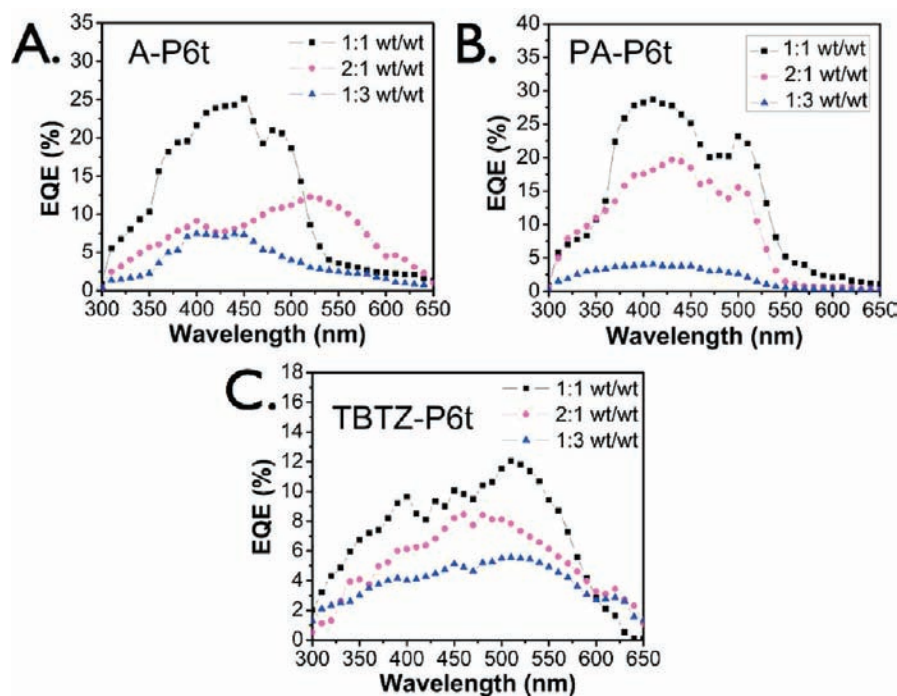


Figure 17. EQE spectra of BHJ donors **A-P6t** (A), **PA-P6t** (B), **TBTZ-P6t** (C) + PCBM; 1:1 wt/wt ratio (black line), 2:1 wt/wt ratio (pink line), 1:3 wt/wt ratio (blue line).

PCBM = 1:3 (maximum EQE \sim 7% at 450 nm). Spectral response data for the **PA-P6t**/PCBM-based OPVs track the progression 1:1 > 2:1 \gg 1:3 (Figure 17B), consistent with the J_{sc} values measured in the corresponding solar cells (2.63, 2.57, and 0.82 mA/cm², respectively). Devices based on semiconductors **A-P6d**, **PA-P6d**, **BTZ-P6t**, **TBTZ-P6t**, and **BTZT-P6t** generally exhibit low EQE responses, except in the case of 2:1 **A-P6d**:PCBM (\sim 10% at 420 nm, Figure S18A), 1:3 **PA-P6d**:PCBM (\sim 15% at 410 nm, Figure S18B), and 1:1 **TBTZ-P6t**:PCBM (\sim 12% at 510 nm, Figure 17C) wt/wt blends.

Conclusions

The design, synthesis, and characterization of a new family of soluble extended arylacetylene optoelectronic materials, **A-P6t**, **PA-P6t**, **BTZ-P6t**, **TBTZ-P6t**, and **BTZT-P6t**, is reported. For comparison, arylvinylenes **A-P6d** and **PA-P6d** were also synthesized and characterized. All of the new extended arylacetylenes exhibit excellent thermal stability. Field-effect transistor measurements demonstrate that all are FET-active, exhibiting significant p-type mobilities. Arylacetylenes **PA-P6t** and **TBTZ-P6t** have well-ordered film microstructures and are the highest mobility p-type materials within this series, with a μ_{th} as high as 0.07 cm² V⁻¹ s⁻¹ and 0.01 cm² V⁻¹ s⁻¹, respectively, under ambient. Organic BHJ solar cells using

PCBM as the electron acceptor were also fabricated with these new extended arylacetylenes. Power conversion efficiencies range from \sim 0.6% to \sim 1.3%. The highest PCE, \sim 1.3% under standard AM 1.5 conditions, is obtained for anthracene-based arylacetylene **A-P6t**. A direct correlation is identified here between OFET hole mobility and OPV performance. These PCEs rank among the highest reported for cells based on nonpolymeric conjugated small molecules. Because the absorption, redox, and film-forming properties of arylacetylenes can be easily tuned, significant advances are anticipated in the near future for this class of semiconductors.

Acknowledgment. We thank MIUR (Ministero dell'Istruzione, dell'Università e della Ricerca, Rome - Italy), DOE (DE-SC0001059) and AFOSR (FA9550-08-1-0331) for support of this research and the Northwestern MRSEC (NSF Grant DMR-0520513) for providing clean room and characterization facilities.

Supporting Information Available: Thermogravimetric analysis (TGA) plots of the arylacetylenes **5** and **7**; UV/electrochemical/FET/OPV data for **1–7**; XRD/AFM images. This material is available free of charge via the Internet at <http://pubs.acs.org>.

JA910420T